2012

Relocation and analysis of the 2007 Nechako, B.C., seismic swarm: evidence for magmatic intrusion in the lower crust

Jesse A. Hutchinson
Western Washington University

Relocation and analysis of the 2007 Nechako, B.C., seismic swarm: Evidence for magmatic intrusion in the lower crust

By

Jesse A Hutchinson

Accepted in Partial Completion

Of the Requirements for the Degree

Master of Science

Geology

Kathleen L. Kitto, Dean of Graduate School

ADVISORY COMMITTEE

Chair, Dr. Jackie Caplan-Auerbach

Dr. Bernard Housen

Dr. Susan M. DeBari

MASTER'S THESIS

In presenting this thesis in partial fulfillment of the requirements for a master's degree at Western Washington University, I grant to Western Washington University the non-exclusive royalty-free right to archive, reproduce, distribute, and display the thesis in any and all forms, including electronic format, via any digital library mechanisms maintained by WWU.

I represent and warrant this is my original work, and does not infringe or violate any rights of others. I warrant that I have obtained written permissions from the owner of any third party copyrighted material included in these files.

I acknowledge that I retain ownership rights to the copyright of this work, including but not limited to the right to use all or part of this work in future works, such as articles or books.

Library users are granted permission for individual, research and non-commercial reproduction of this work for educational purposes only. Any further digital posting of this document requires specific permission from the author.

Any copying or publication of this thesis for commercial purposes, or for financial gain, is not allowed without my written permission.

Signature:_____

Date: _____

Relocation and analysis of the 2007 Nechako, B.C., seismic swarm: Evidence for magmatic intrusion in the lower crust

A Thesis

Presented to

The Faculty of

Western Washington University

In Partial Fulfillment

Of the Requirements for the Degree

Master of Science

by

Jesse Hutchinson

June 2012

Abstract

On October 9th, 2007, a seismic swarm, known as the Nechako swarm, began in south-central British Columbia, approximately 20 kilometers west of the Nazko polygenetic cinder cone. After lasting for well over a month, seismic activity tapered off by November 21st, 2007. This study analyzes data from several temporary broadband seismometers deployed by the Geological Survey of Canada near the epicentral locations of initial events from the swarm. Over 4400 events were observed during this period, from which 1048 absolute locations were calculated, with depths ranging from 26-35 kilometers. All of the events recorded by the temporary seismometers were high frequency, volcano-tectonic earthquakes. A previous study by members of the Geological Survey of Canada reported a b-value (the slope of the magnitude-frequency relationship) of 1.9, indicating magmatic activity as the source for seismic unrest.

Algorithmic double-difference programs HypoDD and TomoDD allowed for precise relocations of earthquake multiplets (earthquakes with similar waveforms) from the swarm, suggesting two distinct spatial and temporal pulses of seismic activity. The first pulse recorded by the temporary seismometers began on Oct. 21st, migrating southeast at a rate of 0.44 km/day from 26.5-28.3 km deep, until Oct. 29th. The second pulse began on Oct. 29th at a depth of 29-31 km, approximately 3 km to the southeast of the first pulse. No clear migration of events between the areas could be observed. On Nov. 2nd the first region of activity resumed seismic unrest. Both regions remained active for the remainder of the swarm. Distinct waveforms and hypocenters from spasmodic bursts (rapidly occurring events with overlapping waveforms) and earthquake multiplet clusters lend further credence to the simultaneous rupturing of the two regions.

The proximity of high-frequency volcano-tectonic events to the crust-mantle boundary (approximately 30 km deep), the presence of spasmodic bursts, high b-value, and two distinct regions of simultaneous seismic activity provide strong evidence that the Nechako swarm was generated by the expansion and propagation of magma in the lower crust. Inverted, nearly identical waveforms are interpreted as originating from the brittle fracturing of solidified magma plugs, driven by the force of magma injection along a dike. From the evidence provided, I have concluded that the two spatially distinct regions of activity are representative of two large sills at the base of the crust, emplaced by crustal underplating, with branching dikes. The swarm was initiated by the brittle failure and fracturing of rock in the lower crust around these regions by either buoyantly rising magma in preexisting sills/dikes, or an injection of new magma from a mantle source.

Acknowledgments

I would like to thank the following people for their contribution and support for my Master's Thesis.

My advisor, Jackie Caplan-Auerbach, for her excellent and enthusiastic support, and to the rest of my committee Susan DeBari and Bernie Housen.

John Cassidy, Hohn Kao, Natalie Balfour, and many more with the Geological Survey of Canada for so kindly donating their waveform data and for providing such a great preliminary paper.

Felix Waldhauser for his feedback and support with HypoDD (and for including me in working with HypoDD v. 2), Jeremy Pesicek for his advice on how to get TomoDD to cooperate, and Celso Reyes for developing GISMO; without which my work would have been much more difficult.

Lastly, I'd like to thank my wife, Lauren Ludwig, and my family, Kathy, Mel, David, and Joe, for their love and support over the years.

Table of Contents

List of Tables

List of Figures

Introduction

Nazko cone is a polygenetic cinder cone located just west of the city of Quesnel in the Nechako basin in south-central British Columbia, Canada (Figure 1), a region that has not had local earthquakes since seismic monitoring began 40 years ago (Cassidy et al., 2011). On October 9, 2007, nearby broadband seismometers (within 200 kilometers) began to record a swarm of earthquakes in the area, which persisted until mid-2008, although the bulk of seismic activity tapered off in late November, 2007. Preliminary analysis by the Geological Survey of Canada showed that during this time hundreds of earthquakes occurred per day, located approximately 30 kilometers west of Nazko cone at a depth of 25-35 kilometers (Cassidy et al., 2011).

In response to the swarm, scientists from the Geological Survey of Canada deployed five temporary broadband seismometers near the region of activity west of Nazko cone (Figure 1). Data were recorded by the temporary seismometers (station names NZ01 – NZ05) from October 20th, 2007 to June 12th, 2008. With the data collected by these seismometers, this thesis further investigates the swarm of earthquakes west of Nazko cone, in the Nechako basin.

This thesis builds upon the initial study by Cassidy et al. (2011) by implementing the data from the temporary seismometers, NZ01-NZ05, for a more detailed analysis of how the swarm progressed. Data from the original study were integrated with the new data set in order to improve analysis techniques. The previous study by Cassidy et al. (2011) was unable to perform a detailed analysis of many of the earthquakes because they were difficult to detect with the more distant broadband seismometers. I have located the hypocenters for events recorded by the locally deployed seismometers, and then relocated the earthquakes using double difference methods (Waldhauser, 2001; Zhang and Thurber, 2003). Using waveform cross-correlation, I have identified and analyzed sets of repeating earthquakes (multiplets), recurring, extremely rapid events known as spasmodic bursts, and clusters of events with inverted waveforms.

By studying waveforms, locations, and temporal patterns of event propagation, a magmatic source for seismic unrest during this time has corroborated the earlier study by Cassidy et al. (2011).

Background

An initial study by Cassidy et al. (2011) inferred that the source of seismic unrest that characterizes the Nechako swarm was magmatic in origin. This conclusion was based on several key factors, mainly the presence of spasmodic bursts, which are rapidly occurring seismic events with overlapping waveforms that have only been associated with magmatic sources (Hill et al., 1990; Sherburn et al., 1998; Hill et al., 2002), and a b-value of 1.9. B-values are the slope of a line of best-fit when comparing the number of earthquakes greater than or equal to a given magnitude on a logarithmic scale, and values higher than 1 are typically associated with volcanic activity because of the greater number of low magnitude earthquakes. Over 800 earthquakes were located from depths of 25-35 km, which Cassidy et al (2011) established as being proximal to the Moho. They compared their results to a similar study of a swarm north of Lake Tahoe in 2004 (Smith et al., 2004), that also proposed a magmatic origin for seismic unrest.

In order to provide a context for this study, I first provide a review of the volcanic, tectonic, and seismic history of the region surrounding the seismic swarm.

Volcanic History

Nazko Cone is one of several volcanic and plutonic features in central British Columbia. Together these shield volcanoes, cinder cones, dikes, and plutons are referred to as the Anahim Volcanic Belt. Spanning 600 km from the western coastline to the east, the volcanic edifices become progressively younger to the east, ranging from 14.5 Ma-7.2 Ka (Bevier et al., 1979; Souther et al., 1987). Ages were determined using K-Ar and radiocarbon dating methods (Bevier et al., 1979, Bevier, 1989, and Souther et al., 1987). The igneous rocks were found to be mainly basaltic in composition with high alkalinities, suggesting an undepleted magmatic source derived from deep within the mantle (Souther et al., 1987).

Nazko Cone, the most prominent and best studied cone in the field, is a small polygenetic cinder cone, the summit of which rises 120 m above the surrounding terrain. Nazko has had at least three eruptions, totaling less than 0.1 km^3 in volume, dated at approximately 340 Ka, 9.0 Ka, and 7.2 Ka (Souther et al., 1987). The first eruptive unit was a subaerial basalt flow. The second unit of basalt erupted during the end of the Fraser Glaciation, and was quenched by the surrounding ice. The third eruption produced tephra, flows, and bombs of basaltic composition. Souther et al. (1987) noted that the alkalinity of the samples decreased over time. Higher alkalinity of the basalts (better classified as basanites) has implied

either decreasing contamination of melt by continental crust or heterogeneities within the mantle source, of which the latter was favored by Souther et al. (1987).

The recent seismic swarm occurred at the eastern extent of the Anahim volcanic belt, nearest Nazko Cone (Figure 1). While Nazko is the nearest volcanic edifice to the initial epicentral locations of the swarm, initial studies indicate that the swarm occurred nearly 30 km deep in the crust and 30 kilometers to the west (Cassidy et al., 2011). Thus, while there is reason to think the swarm was magmatic (Cassidy et al., 2011), it may not have been directly linked to Nazko. Because the linkage between Nazko Cone and the seismic swarm is lacking due to tenuous spatial evidence, I refer to the seismic swarm as the Nechako swarm for this study, after Nechako basin, where the first epicenters were located.

Regional Tectonics, Volcanism, and Magmatism

Rivaling theories have been proposed for the source of the Anahim volcanic belt. Bevier et al. (1979) attribute the source of volcanism to a fixed hotspot reflecting the motion of the west-vergent North American plate. The logic for this argument relies on Sr and Pb isotope ratios, which indicated depletion of radiogenic elements similar to other well-researched hotspot systems, but not as depleted as one might expect from mid-ocean ridge basalt source. A recent tomographic survey revealed a low-velocity zone (P waves slowed by 2%) beneath Nazko cone that extends to nearly 400 km depth and spans several hundred kilometers in width (Mercier et al., 2009), suggesting a large anomaly of mantle origin for the surface volcanism.

In contrast, a study by Thorkelson et al. (2011) suggests that the Anahim belt may be an edge effect of a slab window (Thorkelson and Taylor, 1989) between the subducted Juan de Fuca and Explorer plates. A geochemical transect of British Columbia (Thorkelson et al., 2011) identified Nb/Zr, TiO_2/MnO, and MgO/SiO_2 ratios that were higher than expected of typical continental arc magmatism. Thorkelson et al. (2011) reasoned that the geochemical ratios were indicative of intraplate melting caused by anhydrous asthenosphere upwelling to fill the gap left by the slab window beneath much of British Columbia. They reasoned that the possibility of the magma being generated by a hot spot, extension, or backarc convection should have been ruled out due to the uniform similarity of geochemical ratios along the transect, which they assume would be generally less homogeneous, although the argument was not strongly stated.

Edwards and Russell (1999) assert that without periods of localized extension generated by the motion between the Pacific and North American plates, volcanism would not have been possible in the region.

They do not accept the model of a slab window presented by Thorkelson and Taylor (1989) as the only factor in the most recent (11 Ma – present) volcanic activity. A change in relative plate motion from net compression to net extension between the Pacific and North American plates began nearly 11 Ma (Cox and Engebretson, 1985; Doubrovine and Tarduno, 2008) and ended nearly 4 Ma (Pollitz, 1988). During that time, volcanism became dominantly alkaline, expressing a mantle source, which could have derived from decompression melting (Edwards and Russell, 1999). Since the return to net compression along the plate margin, localized extensional faulting has been attributed to further volcanic activity in much of British Columbia (Edwards and Russell, 1999), although many faults have been inferred and their extent remain to be discovered.

The source of extrusive volcanism in any of the above plate tectonic scenarios is the final component of a complex magmatic process, known as underplating. Picritic (Mg-rich) sills derived from the mantle likely develop near the crust-mantle boundary, and are essentially trapped by the transition between a relatively dense mantle versus a less dense lower crust (Cox, 1980). Over time the magma reservoirs cool, thickening the lower crust.

During the process of underplating, the sills continue to differentiate by fractional crystallization and act as reservoirs for new injections of magma from the mantle (Cox, 1980). After fractional crystallization of denser minerals (e.g. clinopyroxene) occurs, basaltic magma, which is of a lower density than picritic magma, could be potentially forced to the surface by a contrast in its own buoyancy, resulting in flood basalts and other volcanic features (Cox, 1980).

A plains basalt (similar to a flood basalt but on a smaller scale), the Chilcotin Group, underlying much of south-central British Columbia, including Nazko cone, has been associated with back-arc extension and asthenospheric upwelling (Bevier, 1983a). Two eruptive phases from 6-10 Ma to 2-3 Ma (Bevier, 1983b) were found to have compositions typical of melt derived from picritic magmas (Bevier, 1983a). Much of the Chilcotin Group, including cinder cones, is thought to have been scraped away by glaciers since their formation, as evidenced by the exposure of dikes at the surface (Bevier, 1983b). The picritic derived compositions, back-arc extension setting, and style of eruptions (plains basalt) support the case for magmatic underplating in the region.

The eruptions of the Chilcotin Group, and later Nazko Cone, are evidence that the Nechako basin region has had active magmatic sources. If underplating has continued since the past eruptions, then we can hypothesize that the area is underlain by a magmatic system at the crust-mantle transition. In relation

to seismic activity, geophysical properties of underplating within the lower crust and physical attributes of the magma bodies provide the best context for further analysis.

Furlong and Fountain (1986) developed a model to describe the geophysical properties of underplating, which indicated that underplating could cause the continental crust to be thickened in excess of an additional 10 km. P-wave velocities of 7.0 km/s are typically expected for the deepest continental crust, while mantle velocities exceed 7.9 km/s. Furlong and Fountain (1986) calculated that the velocities for a region experiencing underplating would have velocities ranging from 7.1-7.8 km/s.

Jarchow et al. (1993) found the first seismic evidence for magmatic underplating in the Dixie Valley/Carson sink area of the Basin and Range province. Their seismic reflection study revealed that a 200 m thick by 1.8 km long sill lay 31 km below, at the base of the crust. They also calculated that the magma body could be no older than 500,000 years due to its volume and the amount of heat lost due to conduction over time. The depth, age, and presence of this magma body within the Basin and Range has provided evidence for magmatic intrusion in the form of crustal underplating in areas of extension.

Volcano Seismicity

Preliminary observations made by Cassidy et al. (2011) set the stage for this study, showing that the earthquakes expected for the temporary seismometers NZ01-NZ05 would be related to volcanic/magmatic activity. In the following paragraphs, the significance and waveforms of earthquakes related to volcanism are summarized for discussion.

The first classification for volcanic earthquakes was established by Minakami (1974). Three types of earthquakes related to volcanic/magmatic activity in Japan were identified as A-type, B-type, and volcanic tremor (Minakami, 1974). A-type and B-type earthquakes have been studied in much more detail and are more commonly referred to as volcano-tectonic and long period earthquakes (Lahr et al., 1994).

Volcano-tectonic (VT), long period (LP), and hybrid earthquakes recorded at Mt. Redoubt during 1989-1990 eruption represent the three primary types of earthquakes associated with volcanism, and their descriptions by Lahr et al. (1994) have since become the standard in volcano seismicity nomenclature.

Volcano-tectonic (VT) earthquakes are thought to result from brittle failure within rock by stresses induced by magmatic activity, such as dike propagation. These earthquakes have short periods/high frequencies (typically 5-20 Hz) with clearly distinguished P and S waves (Lahr et al., 1994).

The movement of fluids (gas or liquid) within a volcano, such as magma in a dike or water in a hydrothermal system, causes long period (LP) earthquakes. The interaction between moving fluids and the rock walls do not result in brittle failure, therefore the P waves from LP earthquakes gradually emerge from background noise on a seismogram, instead of abruptly, as is the case with VT earthquakes. As the name implies, these earthquakes have long periods/low frequencies (1-5 Hz) (Lahr et al., 1994). They have P-waves that emerge gradually from background ambience on a seismogram.

A third type of earthquake, the hybrid, also observed in the data collected from Redoubt (Lahr et al., 1994; Chouet et al., 1994) is hypothesized to be a mixture of both LP and VT earthquakes. Lahr et al., (1994) suggested that these earthquakes were caused by the brittle failure of a fault, intersecting a fluid body such as a pluton or dike, at first resembling a VT earthquake before taking on LP characteristics.

Volcanic tremors are continuous, low-frequency earthquakes, lasting up to months at a time. Their waveforms typically resemble long-period earthquakes and they generally precede and/or accompany eruptions (Minakami, 1974; McNutt, 1992).

It is possible that seismic activity related to magmatism may not center at the location of the igneous intrusion, but may instead originate on nearby faults reactivated by the intrusion. Intrusions can cause changes in the local Coulomb stress field, which can in turn load nearby faults with stress, triggering slip. These earthquakes are known as distal VT's (Roman et al., 2008).

Repeating earthquakes, or multiplets, are earthquakes with identical waveforms. The shape of a waveform is determined by how a fault fails, where the wave travels, and how it is recorded. If a fault fails in the same way, from the same location, and is recorded at the same seismometer as the failure preceding it, then the two events will appear identical in time series. Multiplets are therefore attributed to repeated failures from the same location. The waveforms of multiplets would subtly change as earthquakes propagate away from the initial event.

Spasmodic bursts are clusters of low amplitude, high frequency earthquakes (4-14 Hz). While an individual spasmodic burst, consisting of tens of events, last only a couple of minutes, hundreds of similar bursts can occur in a few mere hours. They have only been observed with relation to volcanic and volcano-tectonic events (Hill et al., 1990; Sherburn et al., 1998; Hill et al., 2002). Hill et al. (1990) attributes the source of spasmodic bursts to be the rapid failure of double-couple shear faults by a localized increase in fluid pressure induced by magma.

A window into the earthquake source is provided by the b-value; the best fit line of the magnitude of earthquakes when compared to the log of the number of earthquakes of a higher or lower magnitude (Ishimoto and Iida, 1939; Gutenberg and Richter, 1944). For example, a b-value of 1, which is most commonly found for tectonic earthquakes, would have ten times more magnitude 6 earthquakes than magnitude 7 earthquakes. A higher b-value would mean that there are more small earthquakes relative to the number of large earthquakes.

High b-values are expected of earthquakes related to magmatism because the rupture surface area for volcanoes and magma bodies is notably smaller than tectonic faults; therefore earthquakes driven by a magmatic regime have a much greater number of small earthquakes than earthquakes in a region driven by tectonics. High b-values are also associated with higher thermal gradients (Mogi, 1962) and material heterogeneities (Wyss, 1973). Earthquakes caused by regional tectonics typically have b-values of 1, while earthquakes generated by a volcanic or magmatic source typically have higher b-values because of smaller magnitudes and the occurrence of swarms.

Preliminary analyses of the Nechako seismic data by Cassidy et al. (2011) suggested that the events were associated with magmatic activity. The presence of nearby volcanic features (Nazko cone), spasmodic bursts, repeating earthquakes, and high b-values support magmatism as the likely cause for seismic unrest (Cassidy et al., 2011).

Seismic History

After more than forty years of seismic monitoring with no previously recorded earthquakes in the Nechako basin, over 800 earthquakes were observed, using the POLARIS (Portable Observatories for Lithospheric Analysis and Research Investigating Seismicity) regional network, within a three week period beginning October 9th, 2007 (Cassidy et al., 2011). The seismic swarm continued well into early 2008, although the bulk of activity tapered off during November of 2007. The largest earthquake magnitude resolved during this sequence of events was a 2.9, while the majority of the earthquakes in the swarm had very low magnitudes (1 or less; Cassidy et al., 2011). Lower magnitude earthquakes could not be captured by the POLARIS network since the seismometers were not close enough (Cassidy et al., 2011).

An initial study of the data received from the eight regional broadband seismometers (seven temporary stations from the Pacific Northwest Seismic Network and one permanent station from the Canadian National Seismic Network) showed that the earthquakes were located nearly 30 kilometers west of

Nazko Cone, the nearest volcanic edifice, and just south of Narcosli Lake below the Baezeko River, at depths of approximately 25-35 kilometers (Cassidy et al., 2011). The epicenters of these events were used to determine the locations for seven temporary local broadband seismometers, beginning Oct. 16th, which were assigned names NZ01-NZ05 (NZ01 was originally referred to as FPLB), MCMB, and UBRB. UBRB was placed closest to the epicentral locations of the swarm and was the only temporary seismometer analyzed in the original study (Cassidy et al., 2011).

Because of the small size of the events and limited distribution of seismometers, focal mechanisms could not be calculated for most of the swarm events. However, a moment tensor indicative of normal faulting was calculated for one event occurring on Oct. 10th, 17:50 UTC (Cassidy et al., 2011). However, other events recorded at the same stations were noted to have both dilatational and compressional first motions, suggesting that the mode of failure for the events was not strictly normal faulting (Cassidy et al., 2011). Several families of similar earthquakes, or multiplets, were analyzed with data from stations NZ02 and THMB, indicating repeated failures from different locations and/or by different mechanisms (Hutchinson and Caplan-Auerbach, 2010; Cassidy et al., 2011).

Cassidy et al. (2011) used the double-difference location algorithm HypoDD (Waldhauser, 2001) to ascertain more precise hypocentral locations for events from the swarm. From this data, they found that the swarm ranged from 25-31 km depth, but they were unable to distinguish any clear magmatic or fault structures from the shape of the hypocenters. An abrupt termination of the majority of seismic activity at 30 km was interpreted as the approximate depth of the Moho, coinciding with a sharp increase in P and S phase velocities in the velocity model generated by Cassidy et al. (2011). A lateral migration of approximately 0.5 km/day to the southeast was also noted (Cassidy et al., 2011). Location uncertainties were reduced from 1-3 km horizontal and 4-6 km vertical to 0.6 km horizontal and 0.8 km vertical by using relocation methods.

From the initial study conducted by the Geological Survey of Canada, it was noted that the earthquakes were primarily tectonic or volcano-tectonic in nature, with no long period earthquakes or volcanic tremor observed (Cassidy et al., 2011). Some of the earthquakes were identified as spasmodic bursts, a rapid succession of earthquakes caused by sudden fracturing in the deep crust, with locations coinciding with the rest of the swarm. Spasmodic bursts have previously been associated only with volcanic activity (Sherburn et al., 1998), which lends further support to a magmatic source.

Because the swarm was initially thought to be related to Nazko Cone, similar events were sought for comparison. However, few studies can be compared to the events recorded near Nazko Cone because there have not been many seismic swarms recorded beneath monogenetic volcanic fields. A few, such as the swarm preceding the eruption of Cerro Negro volcano in Nicaragua, have been much shallower with fewer earthquakes over a shorter period of time (La Femina et al., 2004). In the case of the Nechako swarm, the swarm did not precede an eruption, nor was it beneath the nearest volcanic feature, Nazko Cone.

Cassidy et al. (2011) noted that a seismic swarm recorded near Lake Tahoe in 2003 was remarkably similar to the Nechako swarm. From late 2003 to early 2004, a swarm of short period earthquakes occurred deep in the crust (as great as 33 km) beneath the northwestern shoreline of Lake Tahoe (Smith et al., 2004). Smith et al. (2004) determined that the seismic activity was caused by the propagation of a dike splitting brittle rock, in part due to the fact that the depths of the earthquakes became progressively shallower to <17 km during November of 2003, with further occurrences at even shallower depths. Smith et al. (2004) concluded that the magmatic intrusion was caused in response to thinning and extension of the crust, rather than a rise of magma along a potential volcanic conduit. Cassidy et al. (2011) did not observe shallowing events, but depths of the earthquakes were similarly near the base of the crust, suggesting a magmatic intrusion as a reasonable source.

Methods

The temporary broadband seismometers were deployed by the GSC following the initial seismic activity in early October. The locations of the five seismometers, NZ01-NZ05, are shown in (Figure 1). The seismometers recorded from Oct. 21st, 2007, until June 13th, 2008 at a sample rate of 100 Hz. The start and end dates for the temporary Nazko stations can be found on Table 1.

Data from the seismometers were recorded by the Geological Survey of Canada. Additional data from the POLARIS network were downloaded from the Earthquakes Canada ftp server. P and S wave arrival time for stations ALRB, CLSB, FLLB, SULB, TALB, THMB, and UBRB were contributed by Natalie Balfour of the GSC. Analysis of Nechako swarm data required the use of a variety of software packages, including Antelope 4.11, MATLAB 2009a, ArcGIS 10, HypoDD (Waldhauser, 2001), TomoDD (Zhang and Thurber, 2003), and the GISMO (GI Seismology Matlab Objects) suite for MATLAB (Reyes and West, 2011). Input files for several programs are listed in Appendix 1, output files for those programs are listed in Appendix 2, and MATLAB scripts written for this study are listed in Appendix 3. Several methods were used to better understand the Nechako swarm, including earthquake locations, event cross correlations, and event relocations.

Event locations were initially determined by measuring the arrival times of P and S phases from a single event at various stations throughout a given area. Phase arrival times are picked based on an estimation of their initial motion, which depends on the eye and judgment of the person picking them. The arrival time results are compared with the predicted values based on a velocity model for the area and are iteratively adjusted until the travel time residual achieves a minimum value. This method is in an attempt to ascertain the absolute location of events.

A catalog of travel time differences between neighboring events can be calculated using the absolute locations and phase picks for events, which is then utilized in double-differential relocation methods. Absolute locations of many events come from the same general source region, but have slightdifferences in travel time when received at a common station. The raypaths travelled by such events are almost identical, so the differences in travel time can be attributed to their spatial offset. By linking pairs of events and their travel time differences at as many stations as possible, the relative locations of events can be improved by an order of magnitude; from kilometers to 100's of meters of uncertainty (Waldhauser and Ellsworth, 2000).

Waveforms from the catalog of located events can be compared to one another in order to determine how similar, or well-correlated, they are. The appearance of a waveform depends on the source's mode of failure, the path travelled by the seismic energy, and the instrumentation that recorded it. Waveforms recorded at the same seismometer, generated by the same mode of failure at the same location, appear identical. Nearly identical waveforms would be the result of events relatively close to one another; a common assumption is that the events occurred within a distance equal to ¼ of a seismic wavelength (Waldhauser and Ellsworth, 2000). Cross-correlated waveforms can be selected based on a minimum correlation coefficient, which is a value for defining the degree of similarity between waveforms. Clusters of events with correlation coefficients exceeding a specific value are considered part of a family of events, also known as multiplets. Highly correlated events have a correlation coefficient of 0.9, which means that they must have at least a 90% similarity to other events within a multiplet cluster. Lower correlation coefficients allow for a broader catalog of events, but their greater dissimilarity results in less precise relative relocations. A catalog of accurate P and S arrival times for events with well-correlated waveforms can be determined using cross correlation, instead of relying on hand-picked arrival times.

The relative locations of events can be further resolved by relocation techniques such as HypoDD, which involve using both catalogs of differential travel times and phase arrivals determined by cross-correlation (Waldhauser, 2001). It should be noted that relocations do not improve the absolute locations of events, which is reliant on the arrival time method.

Below I outline the programs and methods used to determine the locations, cross-correlations, and relocations of the Nechako swarm below.

Locations

Earthquake hypocenters, or locations, were determined using the seismic analysis suite, Antelope. The waveform data from the POLARIS and Nazko networks were examined in order to find the P and S phases of events at multiple stations. Picking multiple phases is paramount in determining the most accurate locations.

Dbpick, an Antelope program, was used to pick P and S wave arrival times for stations NZ01-NZ04 (none were observed at NZ05). Additional picks were made on POLARIS stations to augment those already catalogued by the Geological Survey of Canada. Arrival times for a total of 11395 P waves and 6934 S waves were identified on the combined POLARIS and Nazko networks. Arrival time uncertainties were

assigned depending on how easily first motions could be identified. The data were filtered to frequency ranges of 2-10 Hz and 8-20 Hz. The two pass bands were both used in order to best identify the first motions of P waves, while reducing background noise, for both spasmodic bursts and VT events.

After the arrival times for P and S waves were determined, the Antelope program dbloc2 was used to determine earthquake hypocenters. A simplified version of the velocity structure described in Cassidy et al. (2011) was utilized as a basis for the velocity model used in dbloc2. The combined P and S wave arrival times from the POLARIS and Nazko stations were inverted using a standard algorithm to find the best fit locations, given the assumed velocity model (Table 2). Events with fewer than three P and three S wave arrivals could not be located with any degree of confidence. The final number of located events was found to be 1048, though thousands more were identified but could not be located because their phase arrivals were too small. The absolute locations are provided in Appendix 1.

Relocations

After initial hypocentral locations were determined, additional measures were taken in order to better locate events relative to one another. By using double-difference techniques, which are later described in greater detail, the relative locations of events can be vastly improved upon by calculating travel-time differences and clustering together events with similar waveforms, and by culling out poorly located and outlying events. Two programs were used for this process: HypoDD v. 1 and v. 2 (the primary difference is in using a 2-dimensional velocity model vs. a 3-dimensional velocity model) and TomoDD.

A converter script, called ‘db2HypoDD’, written by Natasha Ruppert of the Geophysical Institute of the University of Alaska Fairbanks, was used to convert the locations from the Antelope database into a format readable by HypoDD and the GISMO suite. The outputted files contain the catalogue of earthquake locations and the arrival times of their associated phases at each station. Ph2dt, a function of HypoDD, reads the arrival times of P and S phases and calculates the travel time differences between like phases (P and P, or S and S) for pairs of events. The output of ph2dt is used as an input to the HypoDD program itself. Several parameters control the output for the catalogue of event pairs and how strongly linked they are considered, including the distance between hypocenters, the minimum number of linked phase pairs, and the number of neighboring events. Strongly linked event pairs, in the case of this study, required a minimum of 6 phase observations per pair.

Using the catalogue of travel time differences among events and the GISMO suite (Reyes and West, 2011) for Matlab, I cross-correlated the waveforms from each event at every applicable station. The

GISMO script, 'dd_make_scp', was used to define the parameters used for cross-correlating, including the frequency range and correlation coefficient. A window of 0.1 seconds before and 3 seconds after the arrival times for P-waves was used to capture the majority of their waveforms, and a window of 0.1 seconds before and 4 seconds after was used to capture the waveforms of the S arrivals. Given the higher frequency nature of the earthquakes, a lower frequency cutoff was set to 2 Hz and the upper frequency cutoff was set to 20 Hz for all situations. Events were correlated with minimum correlation coefficients of 0.5-0.9 in intervals of 0.1 in order to investigate the effects of waveform similarity on earthquake relocations. When executed, the second script, 'dd_process_scp', ran through the catalogue of events, retrieving information from the Antelope database, and generated MATLAB waveform objects for every event at each station, and for both horizontal and vertical channels. The third and final script, 'dd_collate', cross-correlated each waveform object, rejecting any event pairs with correlations less than the minimum correlation coefficient. The cross-correlation data were then output to a data file to be used as input to the double difference location algorithm, HypoDD.

With the catalogue and cross-correlation data files generated, the algorithmic double-difference relocation program HypoDD was used to improve relative hypocentral locations. HypoDD calculates travel-time differences between pairs of events, adjusting the locations of the pairs relative to one another (Waldhauser, 2001) to minimize travel time misfits. The input parameters used for HypoDD relocations are provided in Appendix 1. The layered velocity model developed by Cassidy et al. (2011l Table 3) was used by HypoDD to calculate travel times.

Several attempts at improving hypocentral locations were made by adjusting the weight of cross-correlation and differential catalog data throughout numerous iterations. The absolute locations of the events are emphasized by initially placing a greater weight on the catalogue data. After the absolute locations of the events have been established, the weight of the catalogue data is reduced and the weight of the cross-correlated data is increased to emphasize relative locations of events amongst their neighbors.

HypoDD provides two methods by which earthquake location may be determined. The conjugate gradients method, or least-squares method (LSQR) was used for the iterative process, as opposed to the singular value decomposition method (SVD), which can only relocate small systems of around 100 events. The LSQR method, unfortunately, underestimates location errors (Waldhauser, 2001). The condition number (CND), which is displayed while iterating, expresses the ratio of the largest to the smallest eigenvalue, is recommended to be between 40 and 80 (Waldhauser, 2001). The condition of

the system could be improved by adjusting the amount of damping applied to hypocentral relocations and by increasing the number of cross-correlation and catalogue links per event, so values were adjusted accordingly to produce the best results. Damping values were never raised above 100, as recommended by Waldhauser (2001). The outputted relocations from HypoDD are provided in Appendix 2.

3-Dimensional Velocity Model Relocations

The recently published, detailed velocity model (Cassidy et al., 2011) and the development of two programs, TomoDD and HypoDD v. 2, to calculate relocations in a three-dimensional space led to the decision to implement them into this study in the hopes of producing more precise relative locations, while, in the case of TomoDD, simultaneously inverting for a new velocity model.

TomoDD is a program derived from HypoDD, designed to simultaneously relocate earthquakes using a three dimensional velocity model, and refine the three dimensional velocity model based on the travel time residuals (Zhang and Thurber, 2003). For TomoDD, absolute arrival times are integrated with differential catalog and cross-correlation data sets to produce the best absolute and relative locations (Zhang and Thurber, 2003). In a similar method to that used for HypoDD, priority was first given to the catalogue data for the first iterations, followed by an increase in weighting of the cross correlation data in order to cluster the most similar earthquake hypocenters as precisely in relative space as possible. In order to produce the best three dimensional velocity model, the two dimensional model used by prior investigations (Cassidy et al., 2011) was expanded to cover an area of +/- 120 kilometers in the X and Y directions from the relative epicenter of the swarm, at 52.87° latitude, -124.06° longitude. For the 3d velocity model, a 17x17 grid of nodes extending 17 nodes in the vertical was set up. The spacing, in km, can be seen on Table 4. The outputted relocations from TomoDD are provided in Appendix 2.

With the newest version of HypoDD, HypoDD v. 2 (still in beta testing), a three dimensional velocity model can be implemented to better locate events. Unlike TomoDD, HypoDD v. 2 does not refine the three dimensional velocity; instead it works similarly to the original version of HypoDD, but in a three-dimensional space. The outputted, revised three-dimensional velocity model from TomoDD was used as input to HypoDD v. 2 in order to compare results from the two methods of three dimensional modeling. The outputted relocations from HypoDD v. 2 are provided in Appendix 2.

Results

Event Data and Absolute Locations

I first determined how many earthquakes occurred, and when they occurred, over the entire course of the Nechako swarm. An approximate number of earthquakes were found using the short-term average over the long-term average of waveform amplitude data with the Matlab script 'sta_lta' (Appendix 3). The long term window was 7 seconds, the short term window was 0.8 seconds, and the detection threshold was 2.25. Several other values were tested, but these variables were determined to be the best for acquiring the most real detections while reducing the chances of false detections. At least 4400 earthquakes were detected from October 21st to November 21st on the vertical channel of station NZ02. Because seismic activity began on Oct. 9th, there were at least 800 additional events prior to Oct. 21st that were described by Cassidy et al. (2011). An additional two events on Dec. 13th were observed on stations NZ04, NZ05, and UBRB.

Figure 2 shows the number of earthquakes per day from Oct. 21st until Nov. 21st. The earliest days had the highest amounts of activity, peaking at 668 detected events on Oct. 22nd, with further peaks of activity on Oct. 30th and Nov 2nd, which had 523 and 352 events respectively. Seismic activity on Oct. 21st-23rd and Oct. 29-30th were clearly generated by two distinct phases.

After the station data for NZ01-NZ05 were integrated with the data from the POLARIS network, initial hypocenters were located using dbloc2. 1048 earthquakes were selected and located using 12 stations (Figure 3). Many of the earthquakes had similar waveforms, indicating that they were repeaters (event multiplets). The events occurred beneath an area of over 90 square kilometers, spanning 26-35 km in depth, which delineates a southeastward dipping feature (approximately 36°). The precision of the data was clearly limited by the number of stations; the earliest events have the most poorly resolved locations due to the absence of the temporary (NZ) stations and UBRB, with average errors of 4.17 km, 0.24 km, and 2.24 km in the x, y, and z directions respectively (after the removal of extreme outliers), prior to Oct. 21st.

Immediately following the installation of the temporary stations, the average location errors were reduced to 0.74 km, 0.79 km, and 0.18 km in the x, y, and z directions. The hypocenters clustered more closely and a trend of downward migration with time became apparent. Specifically, hypocentral locations ranged from 15-35 km in depth prior to the installation of the first Nazko stations on Oct. 21st. From Oct. 21st-28th the earthquake swarm moved continuously downward from 26-28 km depth. From

Oct. 29th until Nov. 21st, a second pulse of events migrated to 29-31 km depth, where the majority of activity was centered for the remainder of the swarm. Continuous movement of the swarm was not clear during this time period. Several earthquakes, after Nov. 2nd, occurred at the shallower depths of 26-28 km, concurrent with the deeper activity.

Event Relocations

The 1048 events initially located with dbloc2 were then relocated using HypoDD v. 1 in order to resolve better relative locations. The results from a setup requiring 6 catalogue and 6 cross-correlated observations per event with a cross-correlation threshold of 0.9 yielded 559 relocated events (Figure 4). Pairs of events with cross correlations less than 90% did not meet the minimum number of required observations and were removed from the dataset. Many of the poorly resolved events, especially those before the installation of the Nazko stations, were culled from the dataset by HypoDD because they did not meet the minimum required observations.

The area in which the events locate was reduced to around 36 square kilometers, extending from 26-31 km deep. The downward migration of earthquakes with time can be seen more clearly and the two main pulses of events are more apparent (Figure 5). From Oct. 21st-28th, the majority of events occurred from 26.5-28.3 km depth, gradually migrating downward. The pulse at 29 km depth, observed with the absolute locations, becomes clearer with the relocations, concentrated approximately 3 km southeast of the initial seismic activity, from Oct. 29th until the end of the swarm on Nov. 21st.

Lower cross-correlation thresholds allow for a broader selection of less similar events to be considered for a greater number of relocations. For events with a cross-correlation threshold of 0.8, 597 earthquakes were relocated (Figure A - 1, located in Appendix 4). The distinct clusters visible in Figure 5 merge into a single group (Figure A - 1).

650 events were relocated using the cross-correlation catalogue of events with a cutoff threshold of 0.7 (Figure A - 2). These relocations had even more of an expanded, rounded appearance, making it impossible to interpret any subsurface features (Figure A - 3). At lower cross-correlation thresholds of 0.6 and 0.5, 685 and 751 events were relocated respectively. Any features that could be interpreted using high cross-correlation thresholds were no longer observable.

After examining the initial relocations from HypoDD using a two dimensional velocity model, a three dimensional velocity model was implemented in the program TomoDD. The relocations from a setup

requiring 6 catalogue and 6 cross-correlated observations per event with a cross-correlation threshold of 0.9 yielded 561 relocated events (Figure 6). The resultant relative locations of the earthquakes were scattered when compared to the relocations made using HypoDD. The events ranged from nearly 26-32 km depth, extending across an area of approximately 45 square kilometers. Running TomoDD actually dispersed the earthquake locations over an area greater than the relocations made using HypoDD, which was approximately 36 square kilometers (Figure 7). This is because TomoDD integrates the catalog of absolute locations calculated with dbloc2, in addition to the catalogs of differential travel times and cross correlations, while HypoDD does not (Zhang and Thurber, 2003). Zhang and Thurber (2003) concluded that the absolute location data had little effect on relocations, which seems to be the case for the Nechako swarm as well.

Cross-correlation thresholds of 0.8 and 0.7 respectively yielded 591 (Figure A - 4) and 651 relocated events. As with the HypoDD results, with a cross-correlation threshold of 0.8, the shape of the relocations became less well-defined (Figure A - 5). Relocated events limited by cross-correlation data with a threshold of 0.7 or less lost any trace of distinguishable features (Figure A - 6), once again resembling one large “blob” of events, while having progressively greater location errors. When using cross-correlations of 0.6 or less, the condition numbers for iterations exceeded values of 100, which indicated a poorly conditioned double differential system. Those relocations were not considered sufficient reliable for discussion.

While the relocations proved to be less helpful in clustering similar events together relative to one another, the three-dimensional velocity model was also reconfigured with each iterative step of TomoDD’s process. The final three-dimensional velocity model is show on Figure 8. Very little was changed in the upper portion of the models, but in the 27-30 km range perturbations in velocity across a single depth had differences up to +/- 0.75 km/s. Any raypaths that traced through greater depths would be those that intersected with the more distant POLARIS stations, which had noisy waveforms relative to the Nazko stations. Because the events were fairly well clustered, sufficient ray coverage to do a full velocity inversion was not provided. With higher resolution tomographic surveys of this area it could be possible to determine whether the velocity perturbations shown on Figure 9 are real or a mere byproduct of TomoDD and the POLARIS stations (Figure 10). The initial velocity model reported by Cassidy et al. (2011) was not significantly altered and has been upheld by the results of the revised model.

For the final relocations, v. 2.0b (beta) of HypoDD was used. HypoDD v. 2 works in fundamentally the same way as v. 1.0, but three dimensional velocity models can be used with it. The model outputted by TomoDD was implemented in order to calculate the relocated hypocenters for HypoDD v. 2. While the locations were nearly identical between the two methods, HypoDD v. 2 performed better in clustering together similar earthquake multiplets (Figure 11). As a result, these locations were used for the further analysis of spasmodic bursts and event multiplets.

Relocations using a cross-correlation threshold of 0.9 provided the tightest clustering of data with 559 events. The earliest events from this relocation occurred on Oct. 10th, spanning to Nov. 19th, which nearly encompasses the length of time of the Nechako swarm. The progression from shallower (27 km) to deeper (31 km) events over that period of time was observed (Figure 13). Some of the events from Nov. 4th were observed at approximately 27 km depth, contrary to the general trend of deepening with time.

For relocations using cross-correlation thresholds of 0.8, 0.7, 0.6, and 0.5, the general event locations were nearly the same as with the 2-dimensional model, as were the number of relocated events: 596, 651, 682, and 755 for each of the correlation levels. HypoDD v. 2 locations followed the same general trend as the other location methods: less well-correlated events plotted as clearly less definable shapes.

To discuss the entirety of the earthquake swarm, the lower limit on the number of cross-correlation and catalogue picks required for relocation were set to zero to prevent any initial culling of data. The relocations were made using a cross-correlation threshold of 0.9 and bore a close resemblance in location and shape to the more limited setup prior (Figure 14). 991 events were relocated, 395 more events than previously, which can be interpreted as earthquakes that were not a part of a multiplet family. As can be seen in Figure 15, the range of time covered by the relocated events goes from Oct. 9th to Nov. 18th. The earliest events (Oct. 9th-15th) were the most scattered, preceding the activation of the closest stations (the Nazko stations and UBRB) which shows that the initial events were poorly resolved due to a lack of accurate arrival times and well-correlated waveforms. These observations are corroborated by the absolute location errors, which were much higher prior to the deployment of the Nazko stations, as noted earlier. The same propagation trends, as discussed earlier, were observed once again, although some of the latest events (occurring around Nov. 18th) were more scattered.

Error Analysis

Errors calculated using the SVD (single value decomposition) method are far better constrained than the LSQR (least-squares) method, but are only useful for smaller datasets (Waldhauser, 2001). As a test to evaluate the errors associated with the LSQR results, I used the SVD method on subsets of the Nechako swarm. For the largest multiplet clusters with cross-correlation coefficients of 0.9, 0.8, 0.7, and 0.6, the events were relocated using the SVD algorithm and HypoDD v. 2. The parameters used for the inversion can be found in Appendix 1. The numbers of events relocated and mean error values are shown in Table 5. The errors scale from approximately 50m to 150m for the results in the x, y, and z directions from the hypocenter.

The lowest errors were found using a correlation coefficient of 0.7, most likely due to the greater number of events without being too far removed from one another. Errors for the entire swarm would be made smaller with a larger catalog of events and cross-correlation observations but could not be determined due to the available computational power.

Multiplet Analysis

Event multiplets, from located (and relocated) earthquakes, reveal more about the propagation of the seismic swarm. Highly correlated events with coefficients of 0.9 or higher were broken down into several multiplet clusters. As a reminder, multiplet clusters are groups of events with highly similar waveforms that have very similar source mechanisms and minimal spatial separation. A dendrogram of these events, shows how the most highly correlated events were clustered (Figure 16). Waveforms of the P phase for each event recorded by the vertical channel of station NZ02 were correlated using a time window spanning from 0.1 seconds before their first motion to 3 seconds after their first motion, spanning the entire P-wave and some residual motion, to ensure quality cross-correlation. Because of the high correlation coefficient, the number of events per cluster were relatively limited, with as many as 22 events and as few as 9.

Ten multiplets with the highest correlations on station NZ02 and the largest number of events are shown in Figure 17 along with a histogram showing the dates when the events occurred. The locations of the multiplets (Figure 18), using the HypoDD v. 2 relocations, show that, as predicted, similar events cluster together spatially. Several multiplet clusters initiated concurrently, but were separated by several kilometers of distance, such as clusters 5 and 7. Other multiplet clusters occurred at the same times and in relatively the same locations, but had different waveforms, such as clusters 1 and 3. The earliest clusters (3, 4, and 8) are shallower, approximately 26.5-28 km deep, than the later occurring

clusters (1, 3, 6, 7, and 9), which occurred at depths of approximately 28-29.5 km. Cluster 5 occurred at nearly the same times as the later clusters, but was located in an area closer to the earlier, shallower clusters and cluster 10, which occurred latest in the sequence of events.

In order to conduct a broader analysis of the multiplet clusters, the largest ten multiplets with a correlation coefficient of 0.8 were also examined. In this analysis the number of events per cluster ranged from 38 to 11 (Figure 19). Clusters 2, 4, 8, and 9 were located from depths of 26.5-28 km (Figure 20). The events from clusters 3 and 7 were located from 28-29 km depth and appear distinctly isolated from the other eight clusters. Clusters 1, 5, 6, and 10 occurred at depths of approximately 28.5-30 km, being isolated from the other two groups of clusters. Several events from the multiplets were not relocated close to their well-correlated neighbors, but overall, the multiplet clusters provide further insight into the propagation trends.

As was observed, the clusters can be more broadly separated into three groups spatially and temporally, one shallower and two deeper. The shallowest clusters (2, 4, 8, and 9) also occurred the earliest, from Oct. 20th - Oct. 27th which is consistent with observations of the multiplets with correlation coefficients of 0.9. The first deeper group (clusters 3 and 7) was continuously active from Oct. 25th – Nov. 18th, while the second deeper group (clusters 1, 5, 6, and 10) were only active for a few days, from Oct. 29th – Nov. 2nd. From this information, we can once again see that the earliest events occurred at the shallowest depths, while the latest events occurred at the greatest depths, but also that deepest multiplet clusters can be divided into two broader groups by both their spatial location and their time of occurrence.

Spasmodic Bursts

Spasmodic bursts occur as periods of extremely high seismic activity with waveforms that often overlap in time, making it difficult to distinguish individual events (Figure 21). The days with the highest frequency of spasmodic bursts were Oct. 22nd, 23rd, 24th, 30th, Nov. 2nd, and 6th, which also coincide with the days having the largest number of detected events (Figure 2). A single event from a spasmodic burst, on Oct. 22nd, 8:44:15, was correlated against events throughout the same day to find similar spasmodic bursts. 265 events bore a 70% or higher similarity to the reference waveform, which comprises over a quarter of the total events from Oct. 22nd (Figure 22). 147 events were found to have a similarity of 80% or higher , while 48 were found to have a 90% or higher similarity to the reference waveform. A further 98 events with a 70% correlation were found on Oct. 23rd, but no further dates were found to have well-correlated events relative to this reference event. When looking at a cross-

correlation matrix of the 265 similar events (Figure 23), the earliest events start off with correlations exceeding 80%, becoming less similar, down to 40%, for a short while (approximately 15 minutes), and then more similar once again. This pattern continues throughout the course of the spasmodic burst sequence.

Another period of spasmodic burst activity began on Oct. 29th and continued into Oct. 30th (Figure 24). 132 events were found to have cross correlations exceeding 70%. The event picked for cross correlation analysis within this burst occurred at 13:10:15 on Oct. 29th. Interestingly, the event did not correlate well (< 70%) with the spasmodic burst events from Oct. 22nd, suggesting that these spasmodic bursts occurred at unique locations and represent two different rupturing incidents.

The cross-correlation matrix for the events from Oct 29th-30th shows a clear trend of highly correlated events within segments of time (Figure 25), similar to the Oct. 22nd spasmodic burst. From approximately 3-9 pm on Oct. 29th, the events were mostly correlated at values of 90% or higher and becoming less similar over time.

Spatially, events from the spasmodic bursts that occurred within the same periods of time were located close to one another (Figure 26), within virtually the same range of depths, while events from different periods of time were spatially distinct. The Oct. 22nd spasmodic bursts occurred at approximately 27 km depth, while events from the Oct. 29th-30th spasmodic bursts occurred at approximately 29km depth, consistent with the general trend of migration of the hypocenters during this time period. Later events from the Nov. 2nd and Nov. 6th spasmodic bursts do not appear on the plot because it was too difficult to resolve clear P and S phases at enough stations to determine their locations.

Inverted Waveforms

Upon closer examination of the multiplet clusters selected for a correlation coefficient of 0.9, it was found that the events from clusters 1 (22 events) and 3, (16 events) have similar, but inverted P-waves; where the P-wave in cluster 1 show a compressional first motion, those in cluster 3 show dilatation. When the events in cluster 3 are inverted, however, the waveforms of the p-waves from cluster 1 match almost exactly (Figure 27), with correlations exceeding 90%, while many of the s-waves become inverted (Figure 28), and only have correlations of 30-80%. This phenomena was not unique to merely one station, but was observed for the same events at stations NZ02, NZ03, NZ04, and UBRB (Figure 29), which implies the inverted p-waves were not merely an error in the calibration of the broadband seismometers. The stacked traces for clusters 1 and 3 matches very closely when cluster 3 is inverted.

Waveform inversion were also observed in association with dike injections in Iceland (White et al., 2011) and at Kilauea (Rubin et al., 1998). White et al. (2011) suggested three mechanisms for waveform inversions. Fluid migration could alter the surrounding stress field, causing fractures parallel to a dike or sill to fail as a result (Rubin, 1993). In a second model, solidified plugs within a dike could rupture, sliding forward due to the force of magma behind it; reversals would be caused by whether the top half or bottom half of the dike plug advances forward (White et al., 2011). Finally, dikes could be interconnected by en echelon fractures which could fail in a normal or reverse motion in close proximity to one another (Weinberger et al., 2000).

Discussion

Analysis of the relocations has allowed me to identify that the first seismic events ruptured at approximately 26 km depth on Oct. 9th. By November 21st, the Nechako swarm reached a depth of nearly 31 km. From Oct. 21st-28th events generally propagated 3 km to the southeast and from 26.5-28.3 km deep. From this we can estimate a rate of migration of 0.44 km/day, similar to the estimated lateral migration of 0.5 km/day determined by Cassidy et al. (2011). Following the first pulse of activity, the second pulse initiated on Oct. 29th at approximately 29 km depth. In this second phase no clear trend of migration could be determined, but some events were located as deep as 31 km. Some seismic activity reinitiated on Nov 2nd within the region of the first pulse of activity, concurrent with deeper events, and lasted for the remainder of the swarm.

From these observations, I have established that two spatially distinct regions experienced seismic unrest. Cassidy et al. (2011) reported 30 km as an approximate depth to the Moho and attributed the events to an injection of magma into the lower crust.

The periods of highest activity on Oct. 22nd, Oct 30th, and Nov. 2nd (Figure 2) correspond with the different pulses of activity observed using the relocated events. The first peak on Oct 22nd, totaling 688 events, was also included in the analysis of Cassidy et al. (2011), but the latter two were not observed by them, perhaps due to the small size of the earthquakes. Between each peak, a decline in the number of earthquakes per day can be seen, indicating an initiation of brittle failure, followed by gradual relaxing of the ruptured areas.

Multiplet analysis has shown that several spatially distinct sources ruptured within a short (the same day) period of time. The earliest clusters, from Oct. 20th-Oct. 27th, were the shallowest, often overlapping one another temporally and spatially while retaining distinct waveforms. Similar trends could be seen for the deeper clusters, where two spatially distinct groups of multiplets experienced concurrent activity from Oct. 25th-Nov. 18th. The timing of the multiplets suggests the presence of several sills and/or dikes injecting simultaneously, perhaps due to several independent pulses of magma.

Spasmodic bursts also coincided with the periods of high activity on Oct. 21st-22nd, Oct. 29th-30th, Nov. 2nd, and Nov. 6th. Whether spasmodic bursts are caused by the brittle failure of faults parallel to a dike, motion of a plug of solidified magma, or the rupturing of *en echelon* segments interconnecting dikes (Rubin, 1993; Weinberger et al., 2000; White et al., 2011), they have been directly associated with magmatic activity (Hill et al., 1990; Sherburn et al., 1998; Hill et al., 2002). The events within spasmodic

bursts were found to be well-correlated with correlation coefficients exceeding 0.7, but did not correlate well with events from other spasmodic bursts, which reinforces the model of each burst representing a unique time and place of rapid failure within the crust.

Based on my analyses of the data, spasmodic burst events from Oct. 22nd-23rd alternated between high correlation (> 70%) and low correlation (<70%) approximately every fifteen minutes (Figure 23). Each period of time with highly correlated events could represent highly localized stress, such as along a dike tip, while the less similar events may indicate the rupturing of nearby fractures in response to the altered stress field. This occurred on a slower scale for the events on Oct. 29th from 3-9 pm (Figure 25), which could have been caused by a rupture propagating rapidly within a small area. I propose that the spasmodic bursts are representative of the expansion and propagation of dikes and sills being fed by larger, pre-existing magma bodies.

Nov. 2nd and Nov. 6th were peak days for spasmodic burst activity, which is when the activity at approximately 27 km depth renewed, implying a final shallow pulse of magma before the deepest and latest seismic events. From Oct. 25th- Nov. 18th, two groups of multiplets are interpreted to be the signal of rupture that occurred in spatially distinct regions, implying that two dikes and/or sills formed apart from one another.

Lastly, the observed inverted waveforms, sometimes P and S-waves, and sometimes just the P-waves, further imply a sill/dike network. Three hypotheses have been proposed concerning the mechanism that generates inverted waveforms; coupled faults (Rubin, 1993), rupturing of solid plugs along magma conduits (White et al., 2011), or rupturing of *en echelon* segments connecting dikes (Weinberger et al., 2000). P-waves from cluster 1 had correlations exceeding 90% with the p-waves from cluster 3 after inverting them (Figure 27). The s-waves from both clusters, however, averaged correlations of 50% (Figure 28). Amplitudes of the s-waves from cluster 1 are also much smaller than the amplitudes of the s-waves from cluster 3 (Figure 17). This may indicate rapid attenuation and distortion of the s-waves from cluster 1, which could be caused by interference from travelling through a small body of magma. In this case, the magma plug scenario proposed by White et al. (2011) seems the most plausible, although the hypotheses of Rubin (1993) and Weinberger et al. (2000) should not be discounted, as closely-spaced fracture networks could also cause attenuation. I believe that these sources all provide reasonable explanations for the inverted waveforms and that further analysis by future studies of this phenomenon should be made.

The two spatially distinct regions first highlighted by relocations and then explored in greater detail by analysis of multiplet cluster could be interpreted as at least two large magma bodies with branching dikes/sills (Figure 30), each rupturing the crust while spreading and expanding during magma injection, only to remain quiescent while inactive. Because there was not an initial observed upward migration in seismic activity, I believe that the magma bodies were present before the onset of the Nechako swarm, and that the swarm was initiated either by magmatic differentiation, allowing for less dense magma to exceed lithostatic pressures, or by an injection of new magma from a mantle source, as would be the case in a scenario involving a hot spot or slab window.

The Nechako basin has several possible magmatic sources, including a hot spot (Bevier et al., 1979; Mercier et al., 2009), the edge-effects of a slab window (Thorkelson and Taylor, 1989; Thorkelson et al., 2011), or extension (Bevier, 1983a; Edwards and Russell, 1999). The presence of the Chilcotin Group basalts, derived from a picritic magma source (Bevier, 1983b), as well as the polygenetic cinder cone, Nazko Cone (Souther et al., 1987), in combination with our data and the work of Cassidy et al. (2011), imply that the region has a deep magmatic source. I hypothesize that these events were initiated by the migration and expansion of magma bodies at the base of the crust as a result of underplating (Cox, 1980; Furlong and Fountain, 1986).

Tables

Station	Start Date	End Date
NZ01	Oct. 22nd, 2001, 3:02 AM	Nov. 23rd, 2007, 12:00 AM
NZ02	Oct. 21st, 2007, 12:48 AM	Nov. 22nd, 2007, 12:00 AM
NZ03	Oct. 21st, 2007, 11:31 PM	Nov. 17th, 2007, 12:00 AM
NZ04	Oct. 22nd, 2007, 8:02 AM	July 13th, 2008, 12:00 AM
NZ05	Nov. 23rd, 2007, 10:58 PM	Apr. 16th, 2008, 12:00 AM

Table 1. Start and end dates for stations NZ01-NZ05. The dates are based on when the transmission of waveform data were recorded.

Layer Depth (km)	P-Velocity (km/s)	S-Velocity (km/s)
0.0	4.71	2.72
2.5	4.95	2.86
2.6	6.24	3.6
22.0	7.59	4.38
22.5	5.63	3.25
37.0	7.45	4.3
37.1	8.49	4.9

Table 2. 2-Dimesional velocity model used with dbloc2. This model is a simplified version of the model proposed by Cassidy et al. (2011)

Depth (km)	P-velocity (km/s)
0.0	3.079
2.0	5.917
6.0	5.796
7.0	4.879
13.0	5.588
14.0	6.245
22.0	6.401
23.0	6.245
26.0	6.747
27.0	6.920
28.0	7.180
29.0	7.439
30.0	7.958
33.0	7.958
36.0	7.985

Table 3. 2-dimensonal velocity model used for HypoDD. The given velocities are of p-waves, which are approximately 1.73 times the velocity of s-waves (Cassidy et al., 2011).

X	-240	-12.0	-10.0	-8.0	-6.0	-4.0	-2.0	-1.0	0.0	1.0	2.0	4.0	6.0	8.0	10.0	12.0	240
Y	-240	-12.0	-10.0	-8.0	-6.0	-4.0	-2.0	-1.0	0.0	1.0	2.0	4.0	6.0	8.0	10.0	12.0	240
Z	-50	0.0	2.0	6.0	7.0	13.0	14.0	22.0	23.0	26.0	27.0	28.0	29.0	30.0	33.0	36.0	340

Table 4. Grid node spacing of the 3-d velocity model (km) used for TomoDD and HypoDD v. 2. The velocity structure reported in Table 2 by Cassidy et al. (2011) was applied to the grid. The 3-d velocity input has been included in Appendix 1, and the revised velocity model generated by TomoDD has been included in Appendix 2.

CC Coefficient	# of Events	ex (m)	ey (m)	ez (m)
0.9	16	99	110	126
0.8	31	62	69	109
0.7	39	58	57	87
0.6	65	111	83	157

Table 5. Error results for relocated earthquakes using the SVD method with HypoDD. ex is the uncertainty along the x-axis, ey is the uncertainty along the y-axis, and ex is the uncertainty along the z-axis.

Figures

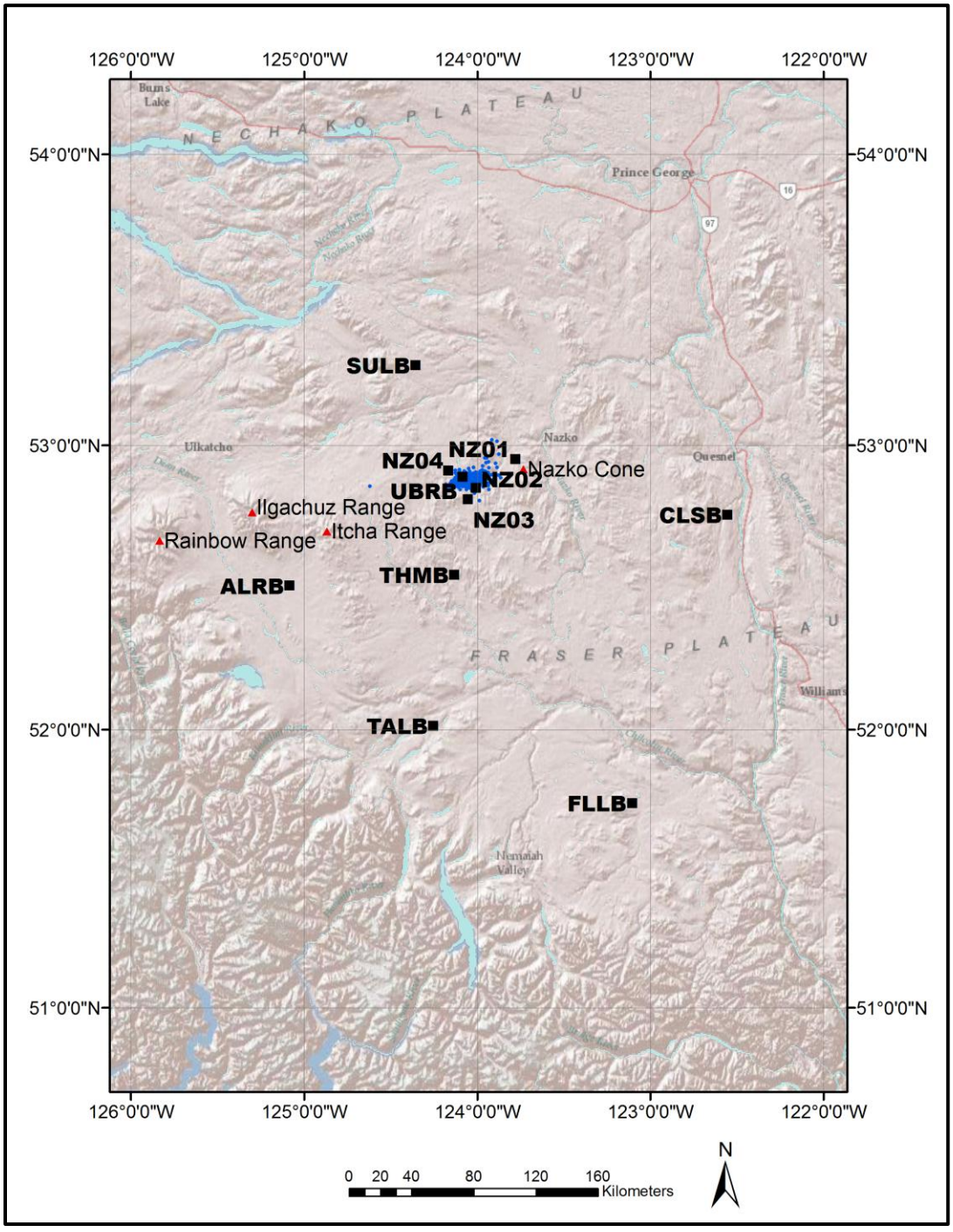

Figure 1. Map of the study area. All stations shown provided data for this study. NZ01-NZ04 were not analyzed in the study by Cassidy et al. (2011).

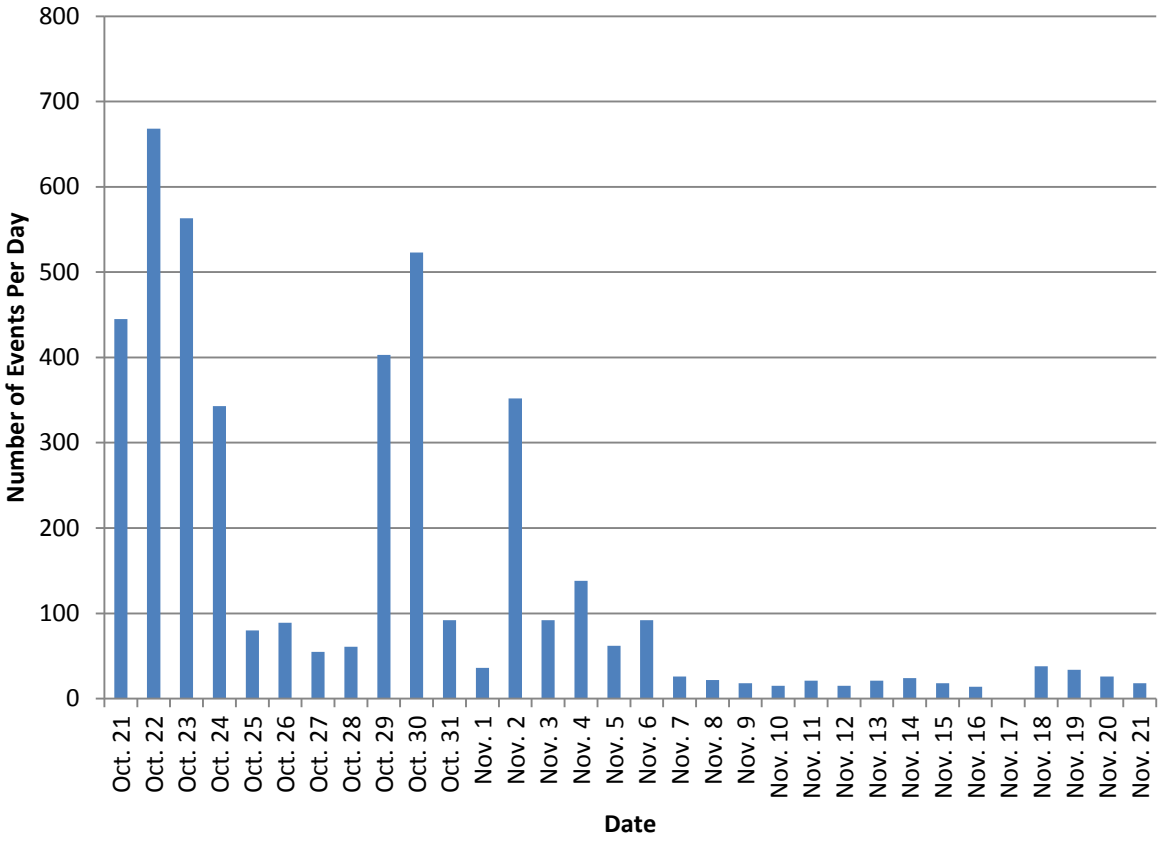

Figure 2. The number of events per day for the Nechako swarm, as detected by using a short term over long term average ratio for the waveform data of station NZ02. Oct. 21st-23rd and Oct. 29th-30th show two distinct pulses of seismic activity. A third but less energetic pulse initiated on Nov. 2.

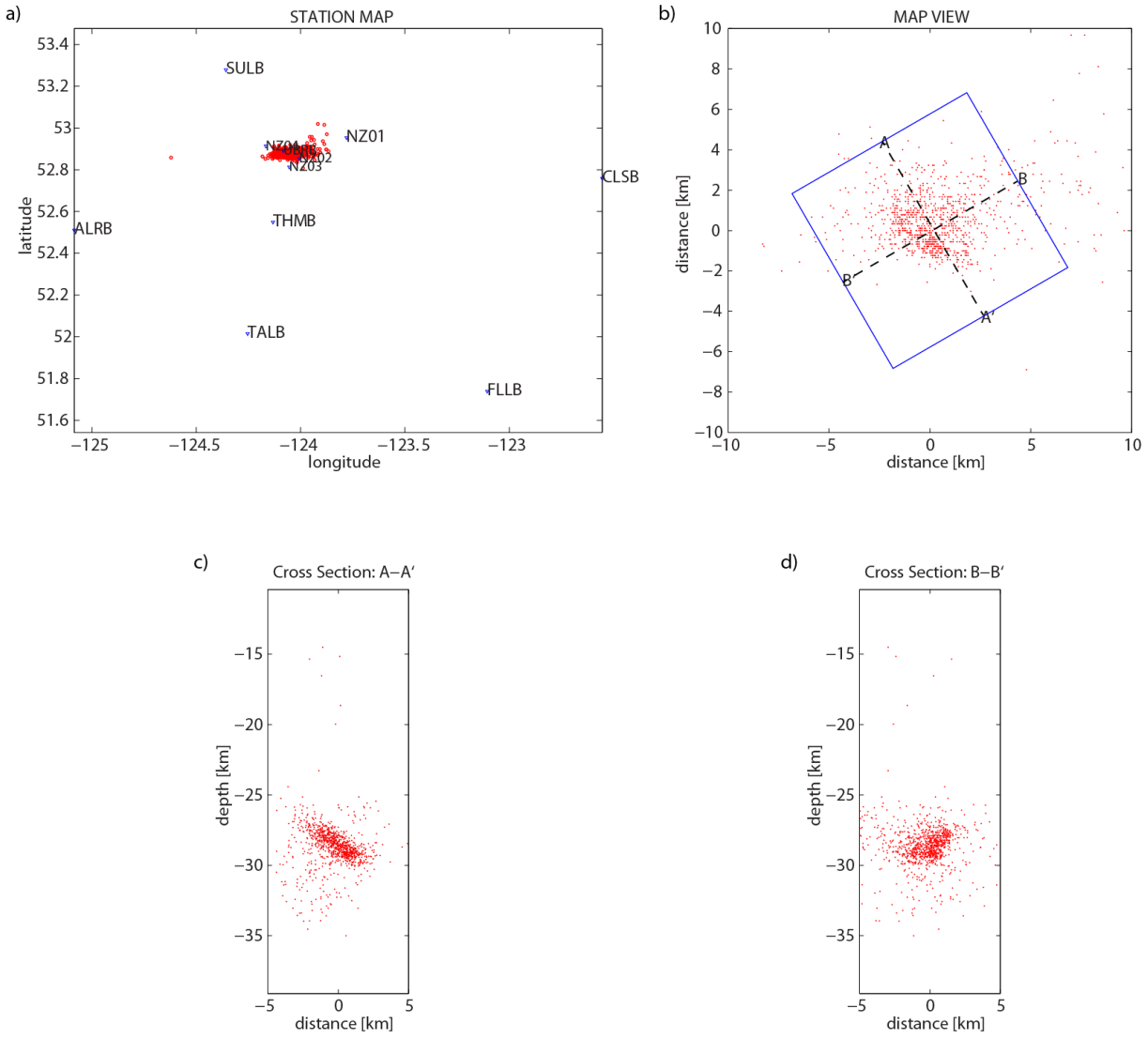

Figure 3. a) Epicentral locations relative to the POLARIS and temporary stations. These locations were calculated with dbloc2 using the combined NZ and POLARIS station data. b) Close-up view of epicenters. The section lines show the orientation of the cross sections in figures 3c and 3d below, which display the events within the blue box in figure 3b.

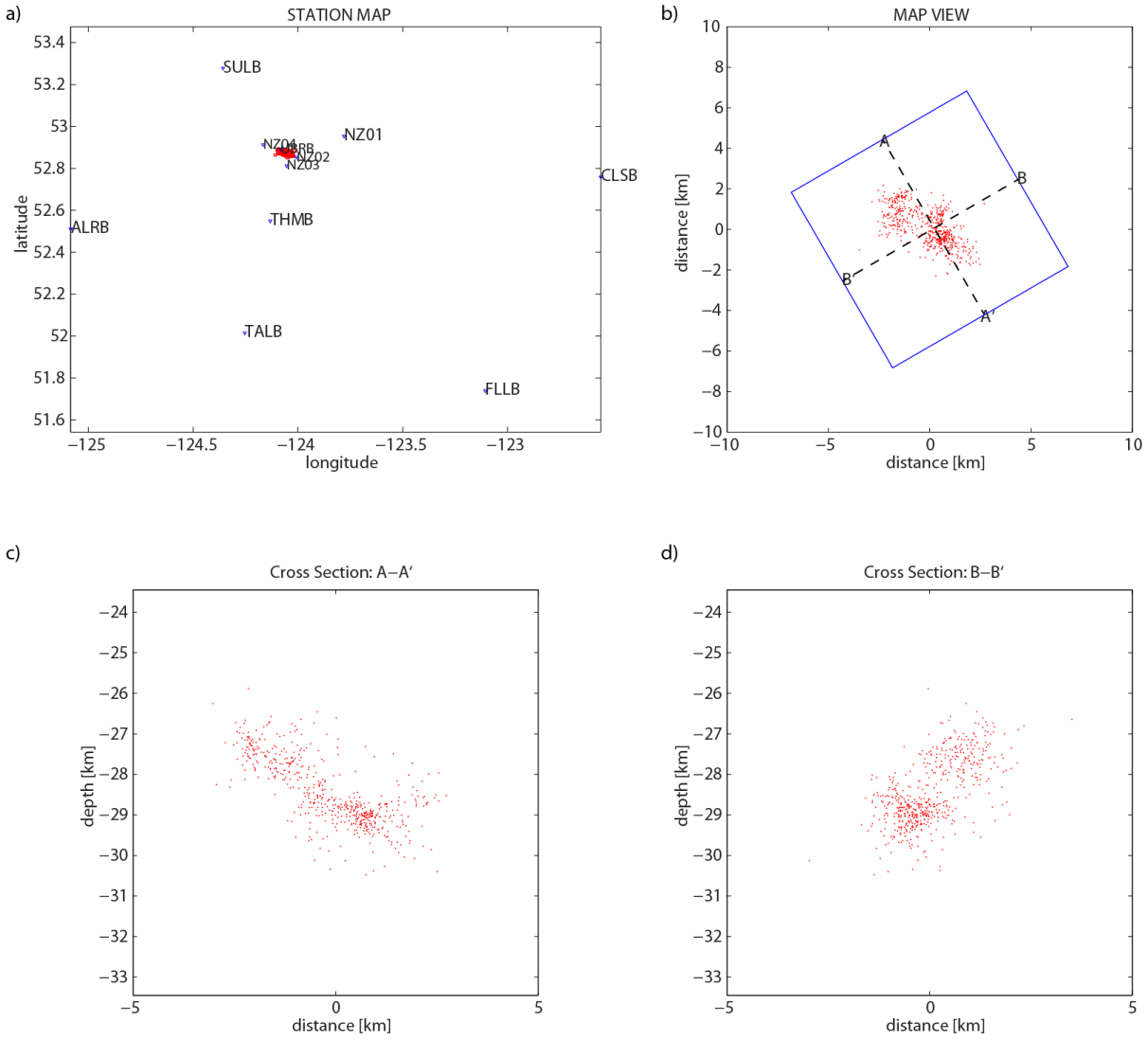

Figure 4. a) Epicentral relocations relative to the POLARIS and temporary stations. Relocations were calculated using HypoDD v. 1 and a catalog of cross-correlations with a coefficient of 0.9. b) Close-up view of epicenters. The section lines show the orientation of the cross sections in figures 4c and 4d below, which display the events within the blue box in figure 4b.

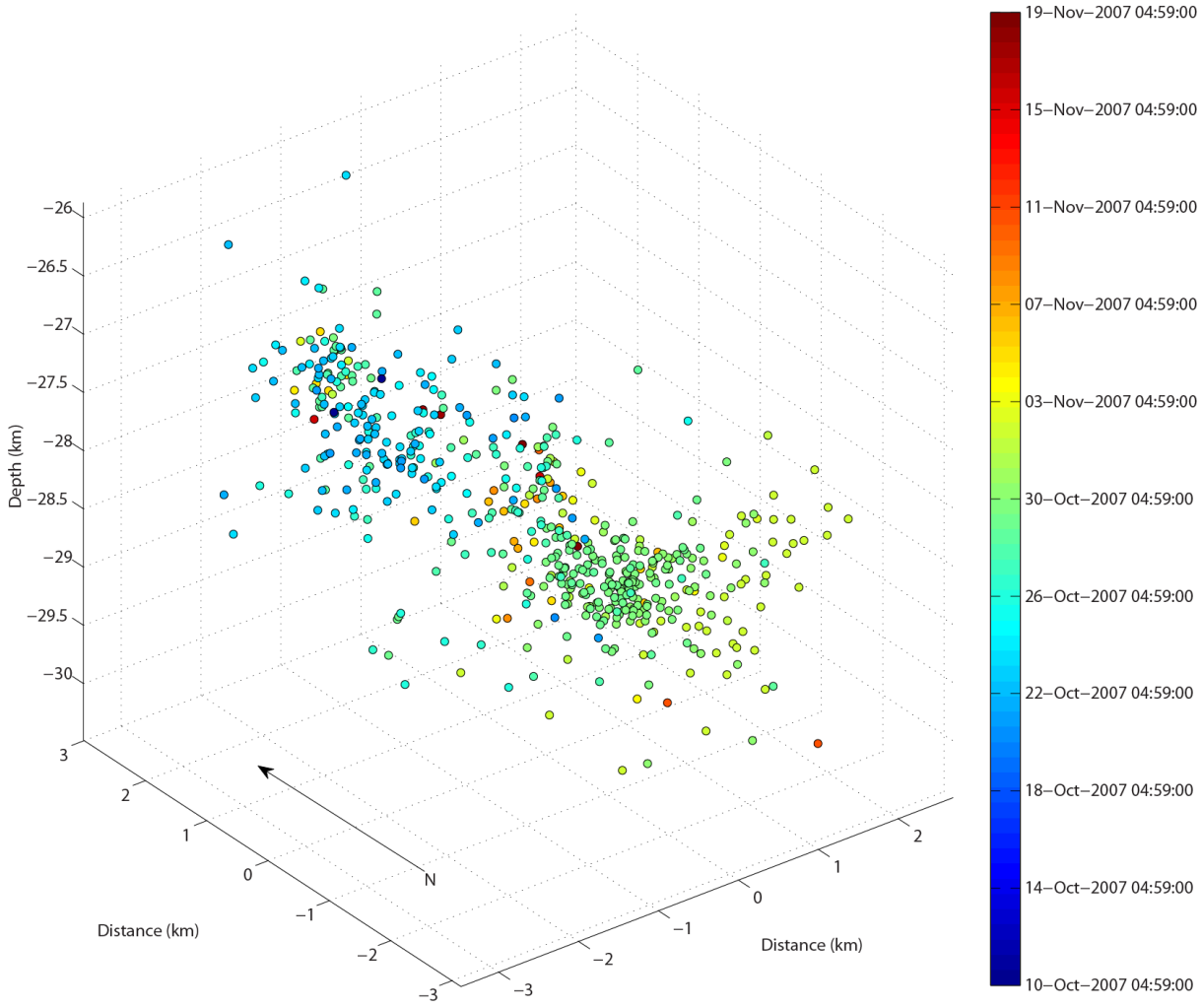

Figure 5. Time series plot of earthquakes relocated in HypoDD v. 1 (Figure 4). Cooler colors represent earlier activity and warmer colors represent the later stages of the swarm.

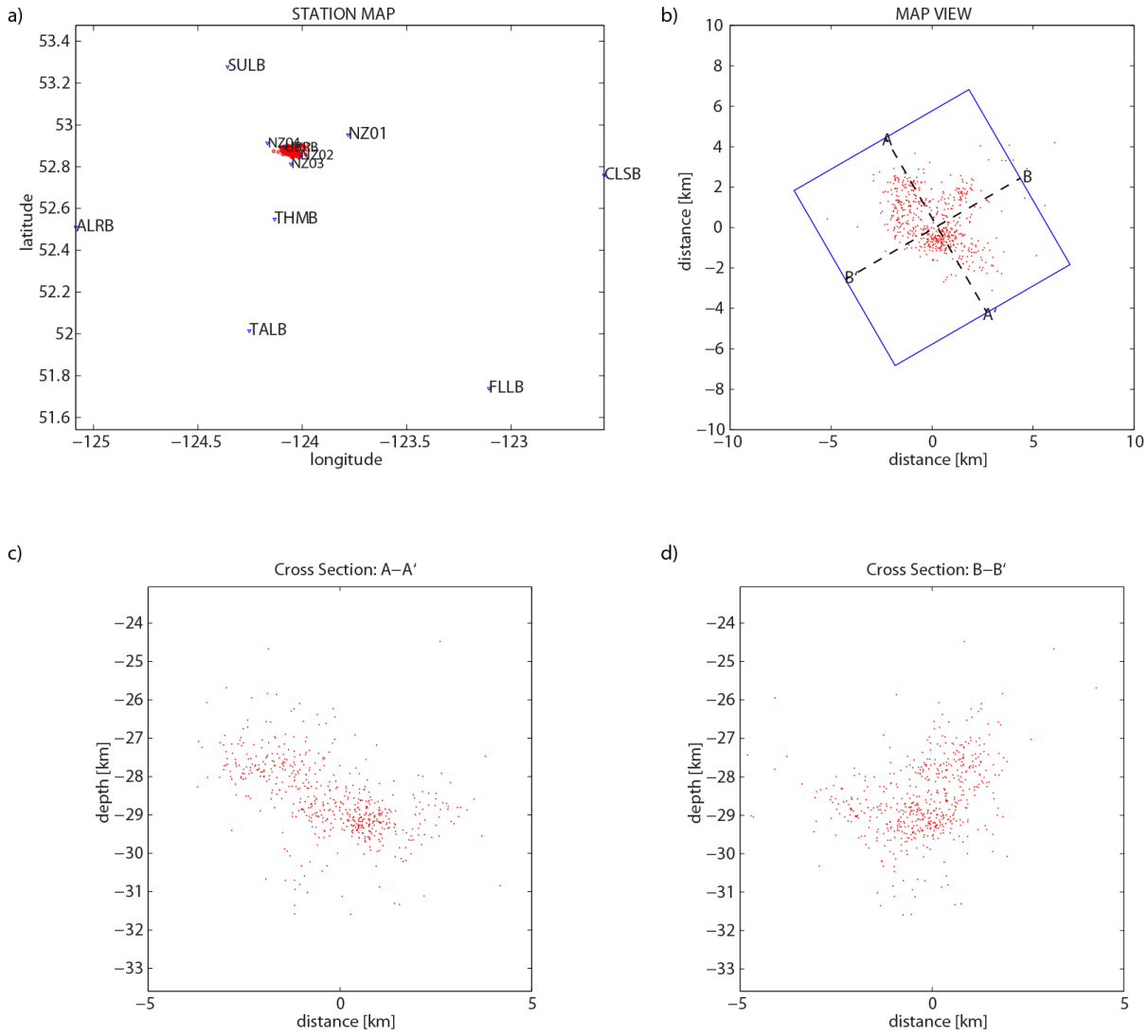

Figure 6. a) Epicentral relocations relative to the POLARIS and temporary stations. Relocations were calculated using TomoDD, a 3-dimensional velocity model derived from the model published by Cassidy et al. (2011), and a catalog of cross-correlations with a coefficient of 0.9. b) Close-up view of epicenters. The section lines show the orientation of the cross sections in figures 6c and 6d below, which display the events within the blue box in figure 6b.

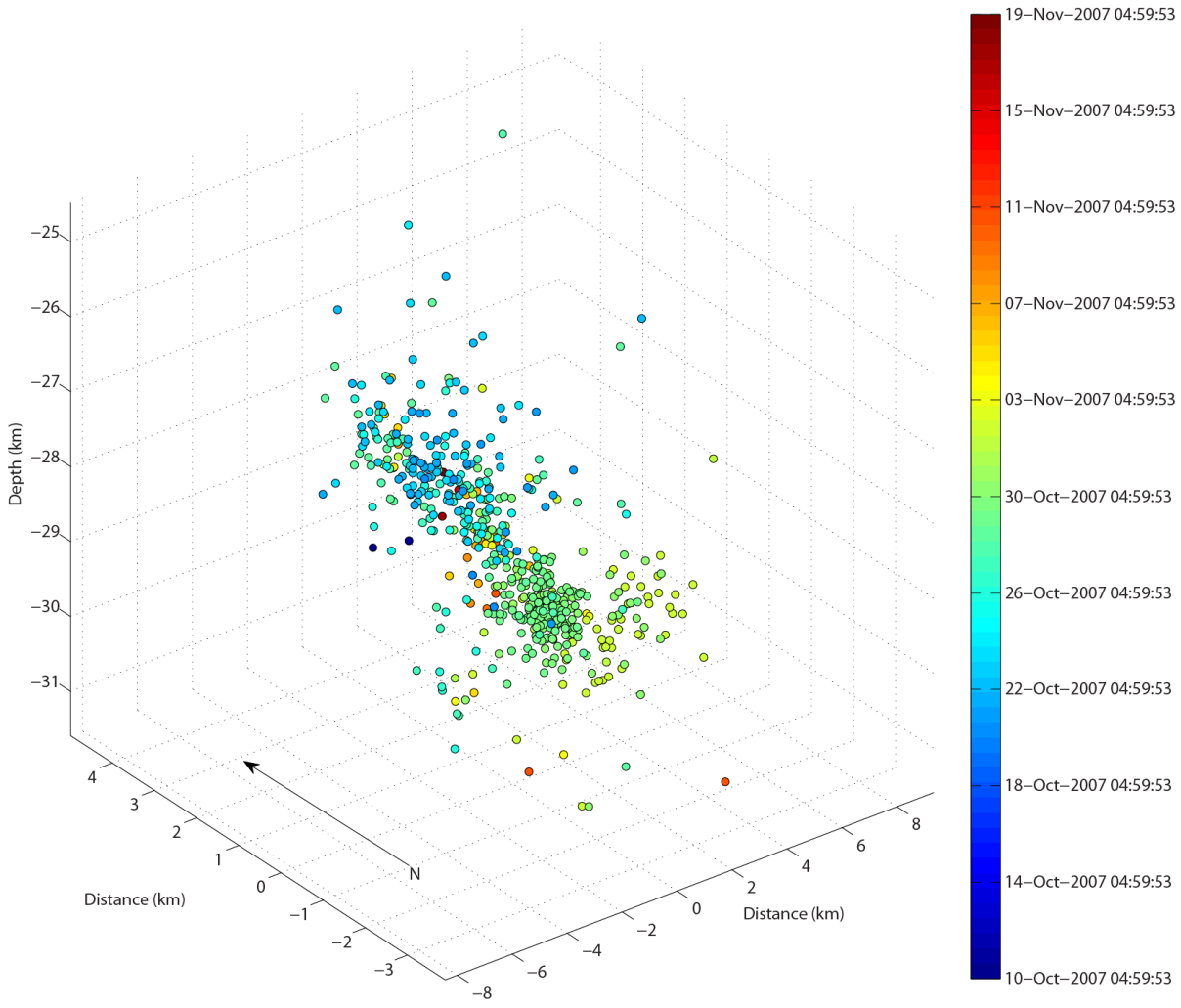

Figure 7. Time series plot of earthquakes relocated in TomoDD (Figure 6). Cooler colors represent earlier activity and warmer colors represent the later stages of the swarm.

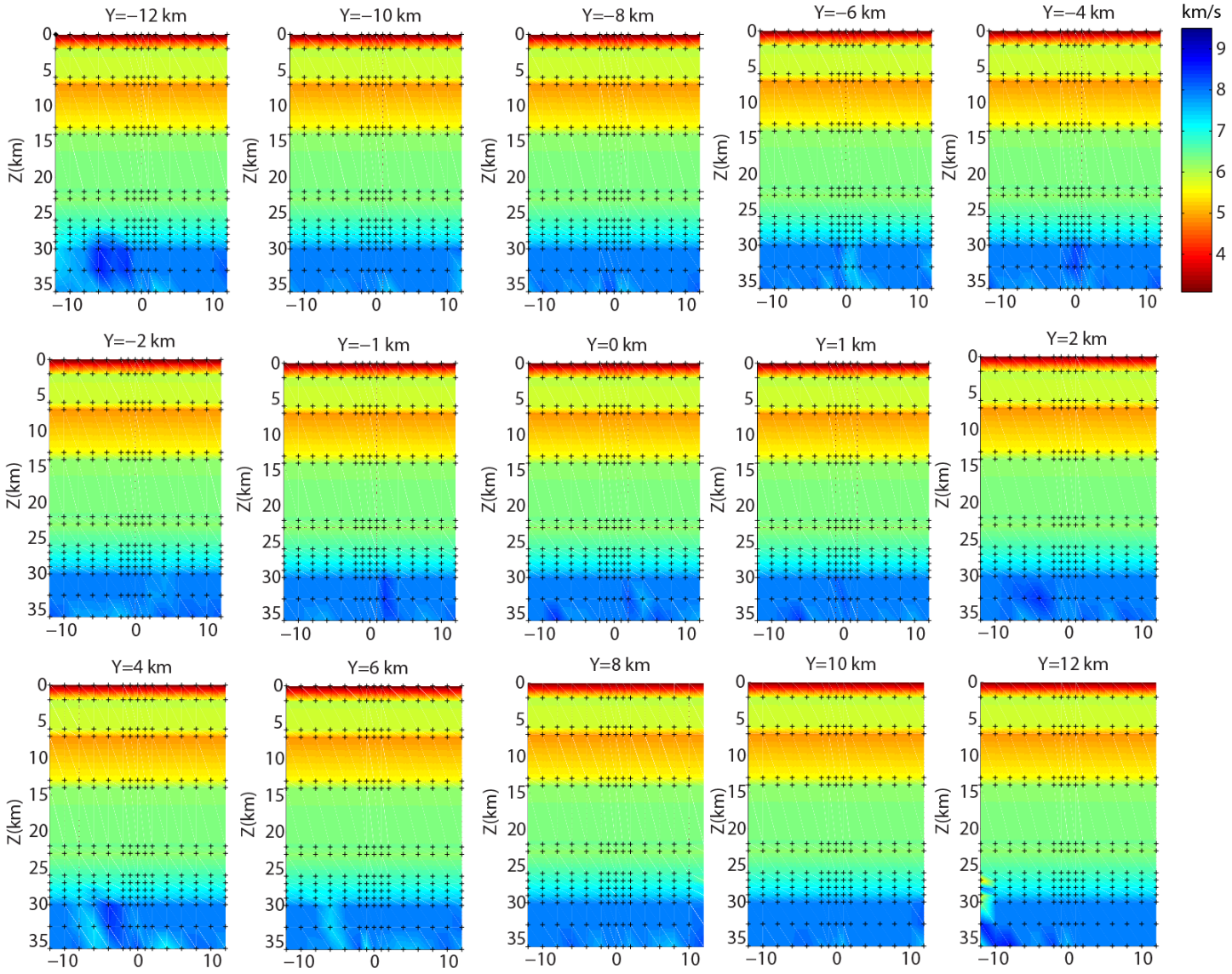

Figure 8. Revised 3-dimensional velocity model generated with TomoDD, derived from the 2-dimensional velocity model published by Cassidy et al. (2011). Each graph is a vertical cross-section through the Y-axis (north/south) in relation to the center of the velocity model. The color bar shows P-wave velocities in km/s. Cool colors are faster velocities and warmer colors are slower velocities.

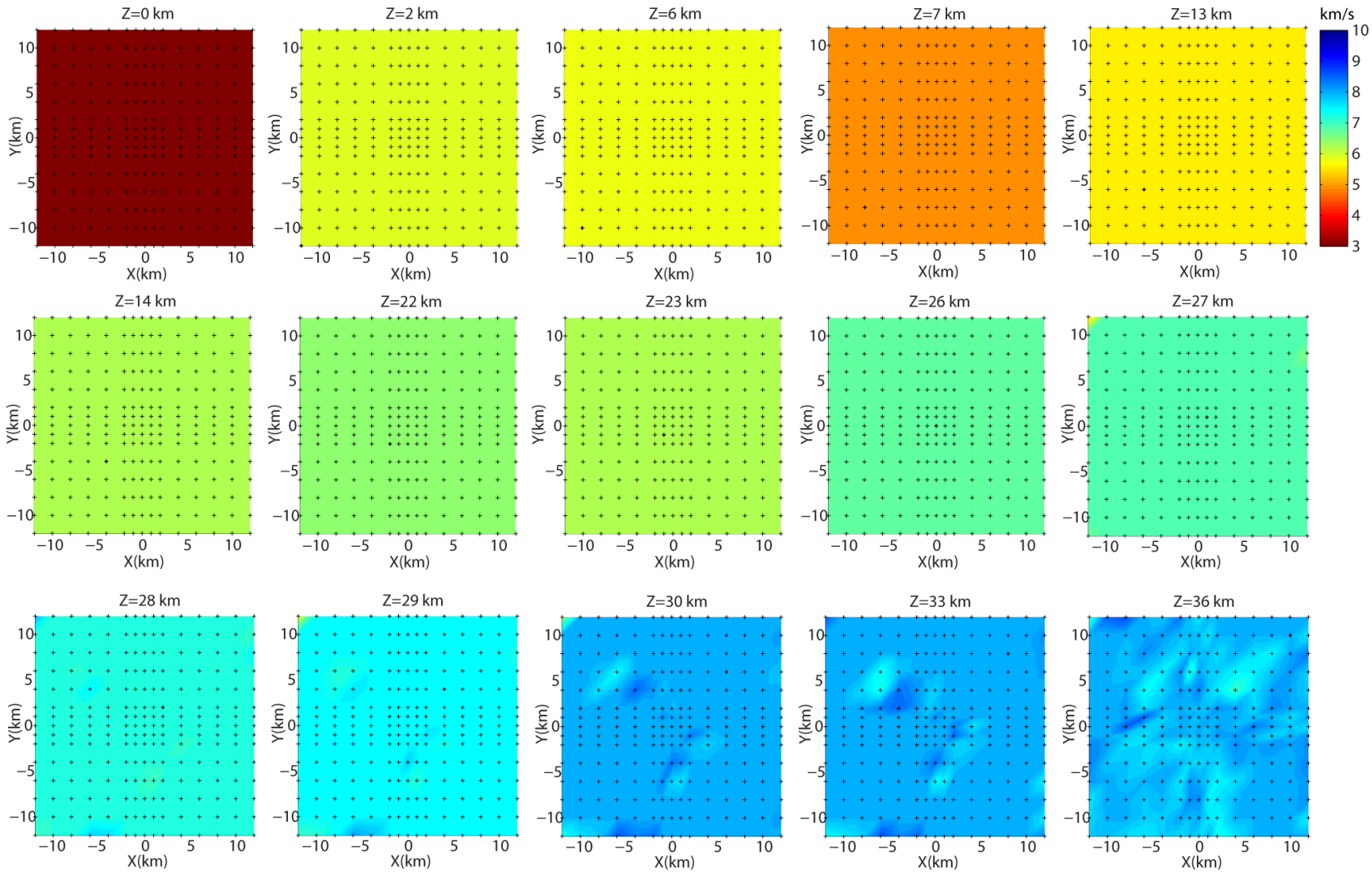

Figure 9. Revised 3-dimensional velocity model generated with TomoDD, derived from the 2-dimensional velocity model published by Cassidy et al. (2011). Each graph is a horizontal cross-section through the Z-axis (depth). The depth is given in relation to the surface. The color bar shows P-wave velocities in km/s. Cool colors are faster velocities and warmer colors are slower velocities.

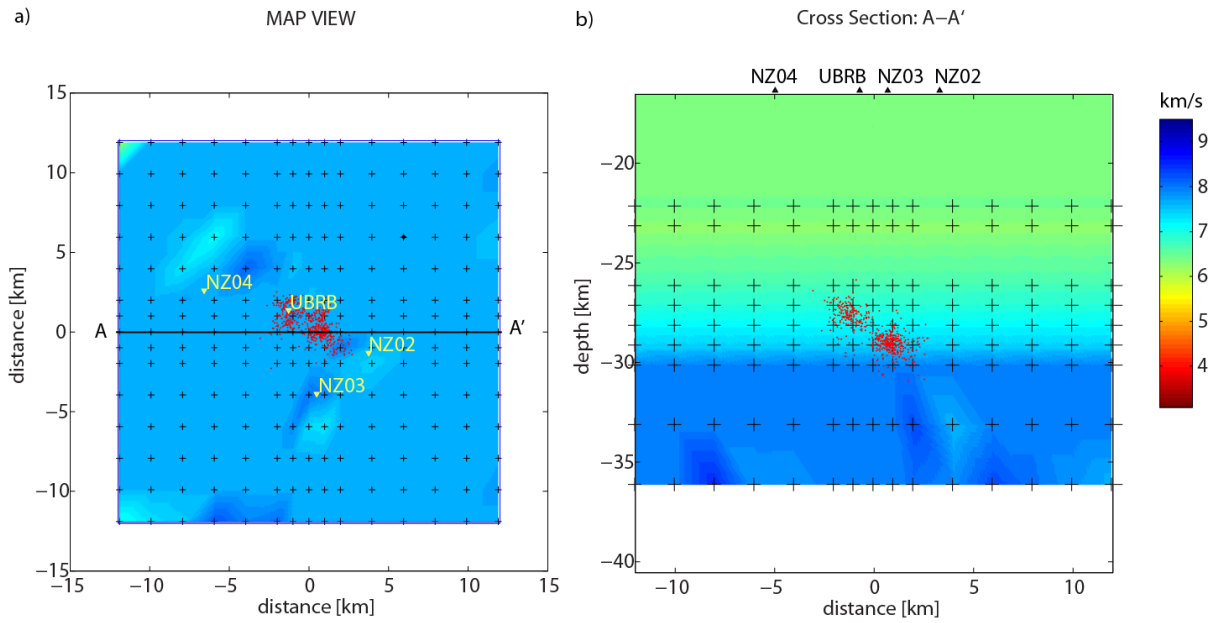

Figure 10. a) Epicentral relocations calculated using HypoDD v. 2 and a correlation coefficient of 0.9 overlaying the horizontal cross-section of the revised 3-dimensional velocity model at 30 km depth. Line A-A' shows the orientation of the cross-section in 10b. Note that the raypaths to the local seismometers for the majority of the events would not travel through the regions of the velocity model showing perturbations. Those phases that would have travelled through the anomalous deep features would have reached the more distant POLARIS seismometers. The color bar shows P-wave velocities in km/s. Cool colors are faster velocities and warmer colors are slower velocities.

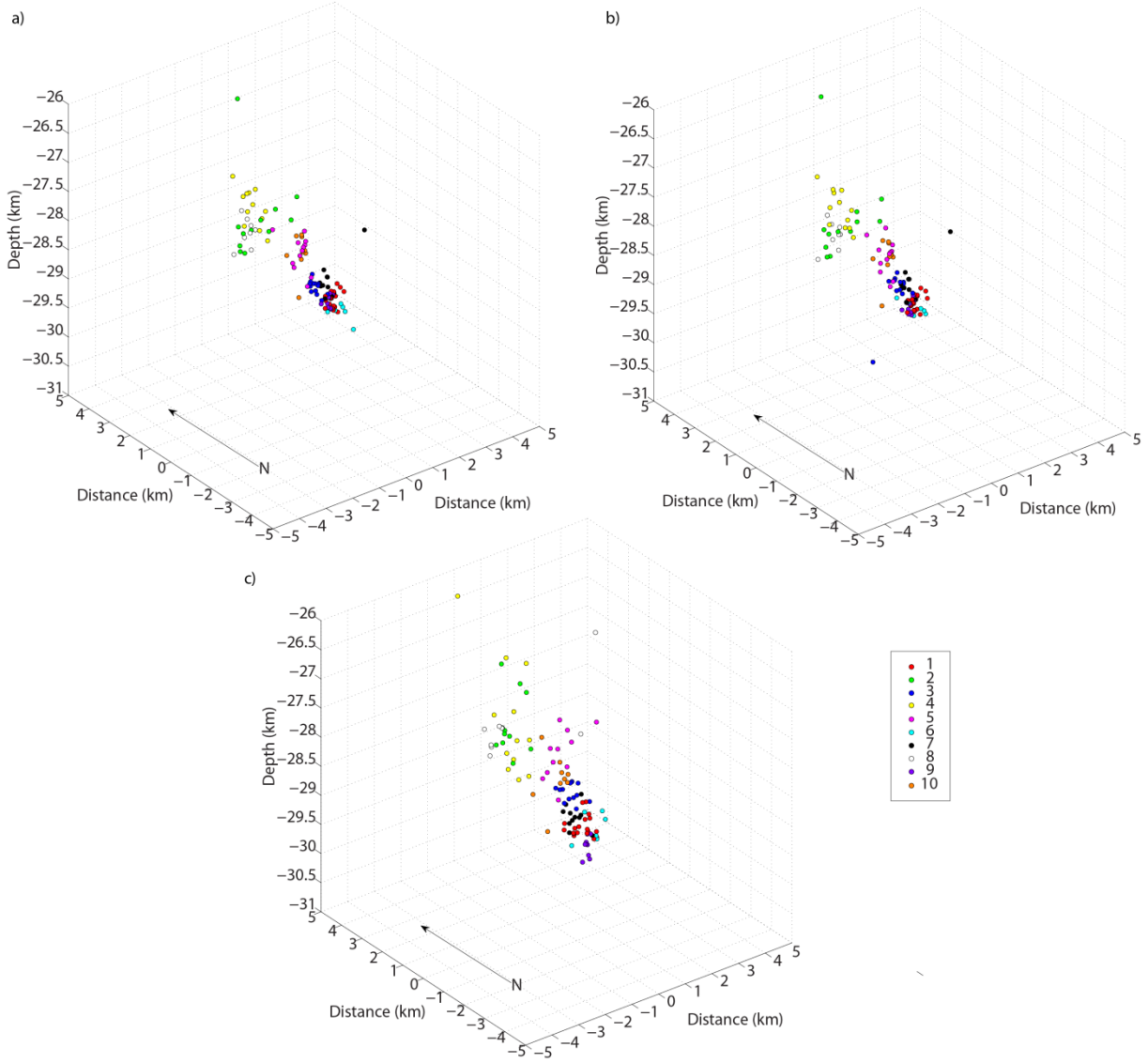

Figure 11. A comparison of relocations with multiplet clustering using a) HypoDD v. 2, b) HypoDD v. 1, and c) TomoDD. Multiplet clusters shown are the then largest clusters of events with correlations of 0.9 or higher. When using the data from TomoDD, clustering appears the least tight, while HypoDD v. 1 and v. 2 are both very similar. The relocations from HypoDD v. 2 show slightly tighter clustering for the majority of event multiplets, so these relocations were chosen for later discussion of the results.

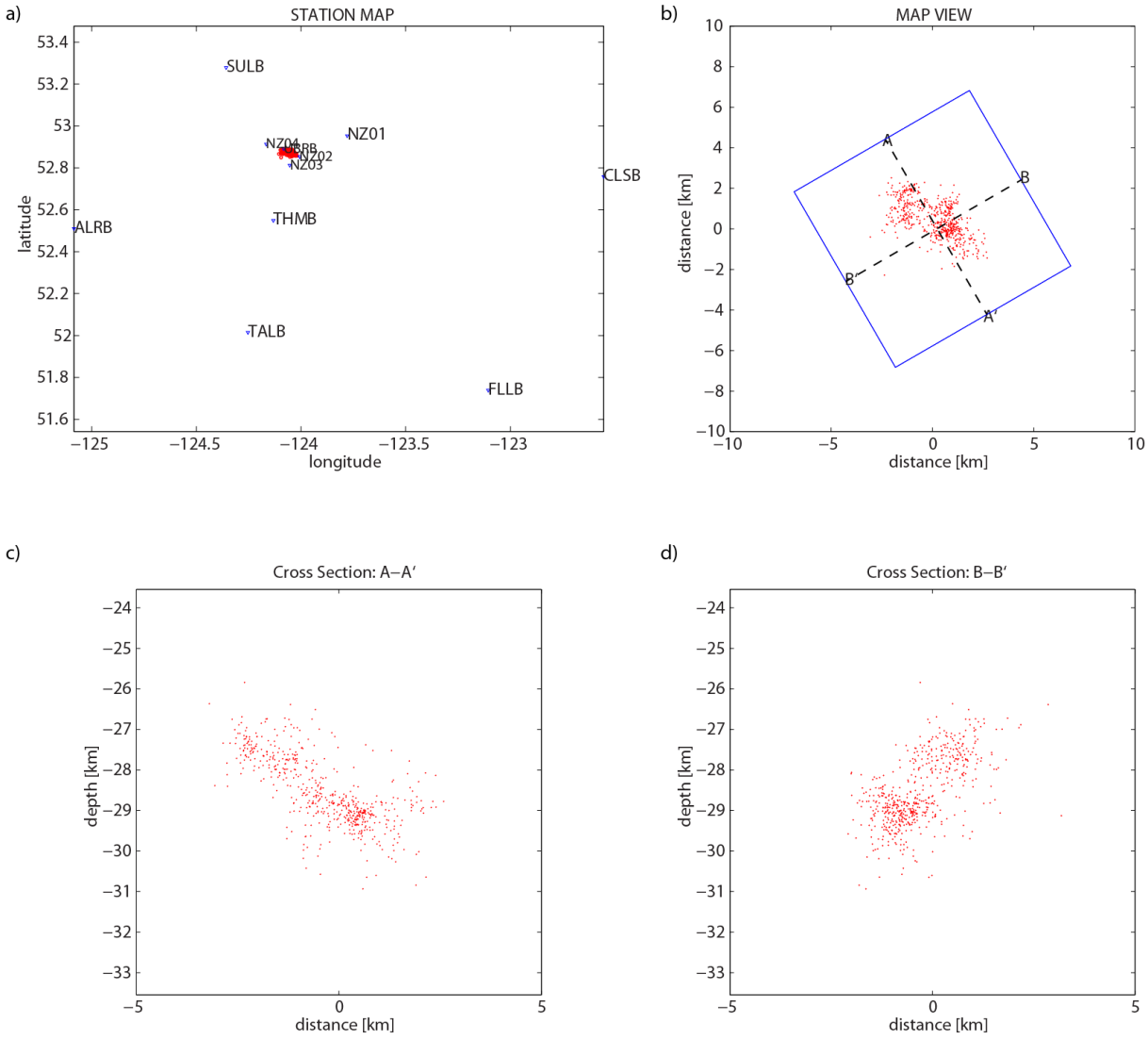

Figure 12. a) Epicentral relocations relative to the POLARIS and temporary stations. Relocations were calculated using HypoDD v. 2, the revised 3-dimensional velocity model, and a catalog of cross-correlations with a coefficient of 0.9. b) Close-up view of epicenters. The section lines show the orientation of the cross sections in figures 12c and 12d below, which display the events within the blue box in figure 12b.

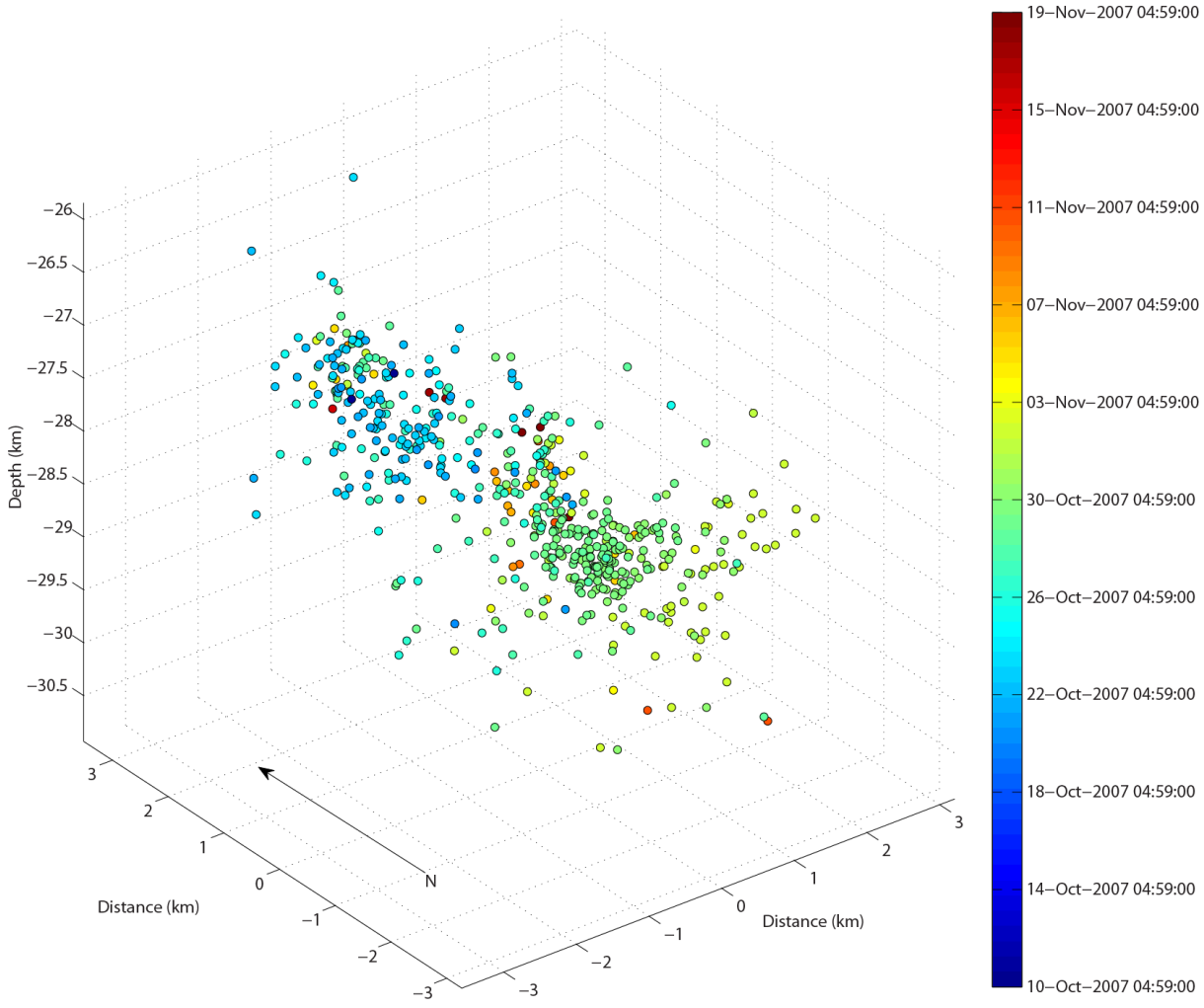

Figure 13. Time series plot of earthquakes relocated in HypoDD v. 2 (Figure 12). Cooler colors represent earlier activity and warmer colors represent the later stages of the swarm.

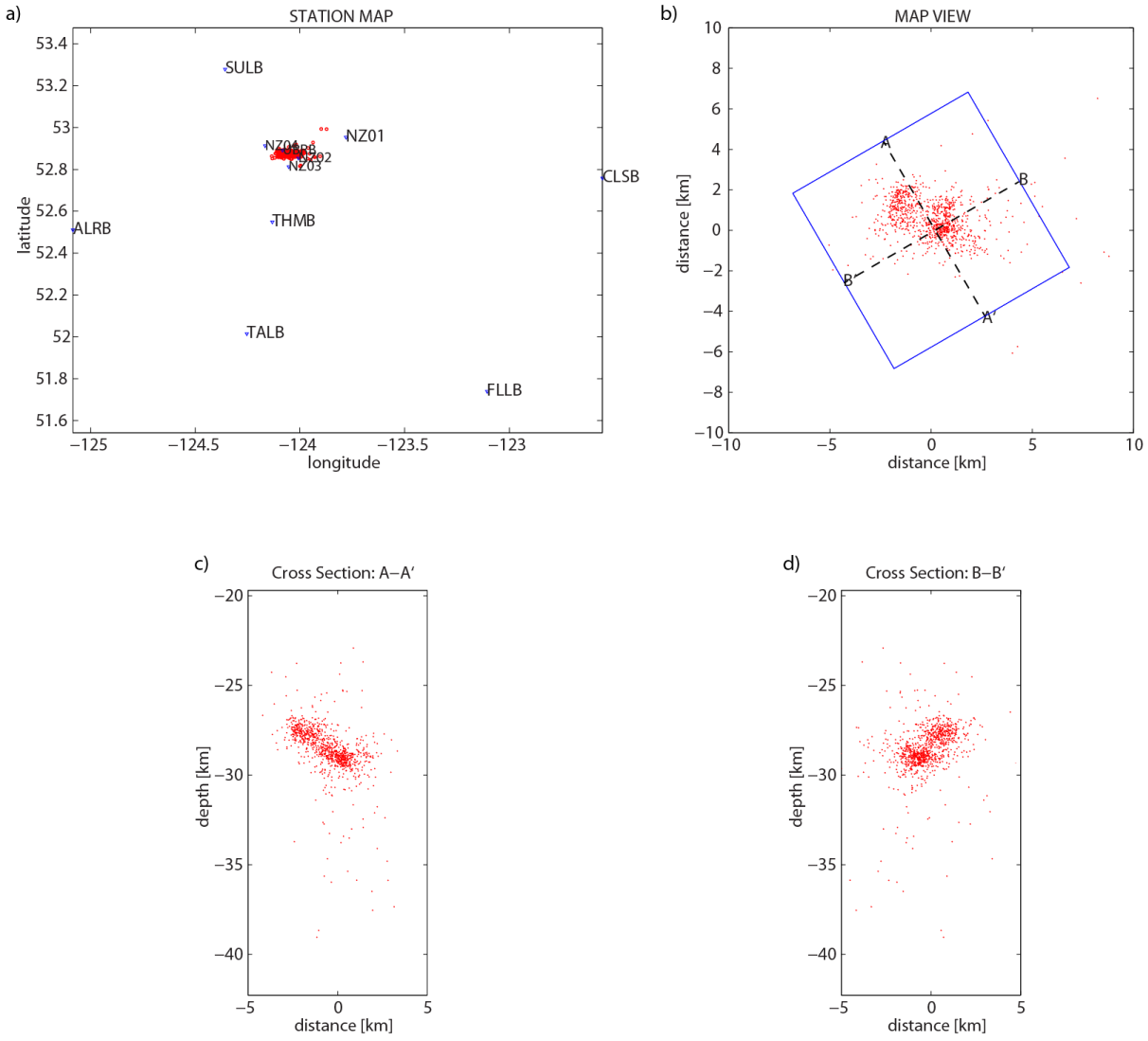

Figure 14. a) Epicentral relocations relative to the POLARIS and temporary stations. Relocations were calculated using HypoDD v. 2, the revised 3-dimensional velocity model, and a catalog of cross-correlations with a coefficient of 0.9. No lower limits to the number of catalog and cross-correlation observations were used for these relocations. b) Close-up view of epicenters. The section lines show the orientation of the cross sections in figures 14c and 14d below, which display the events within the blue box in figure 14b.

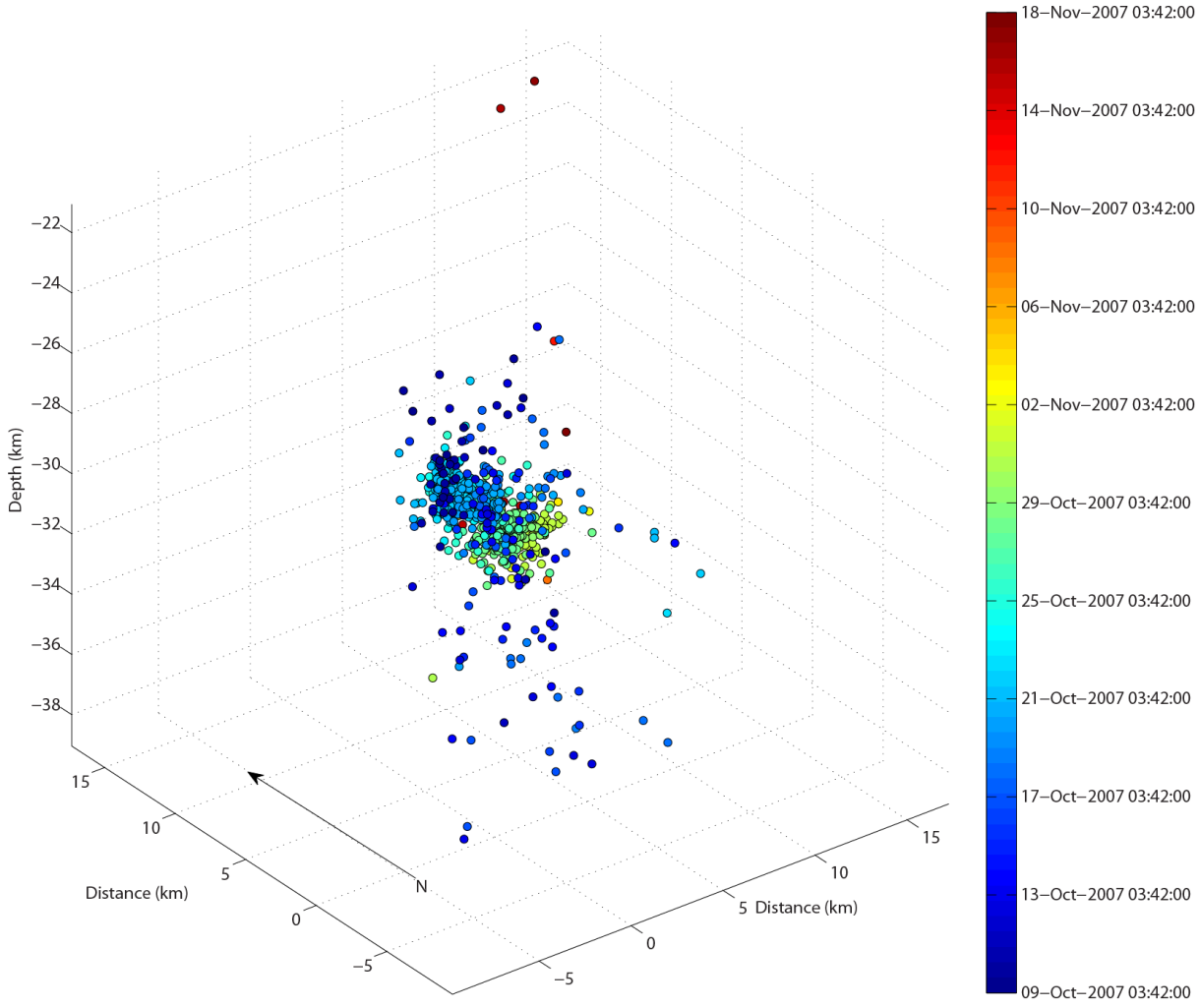

Figure 15. Time series plot of earthquakes relocated in HypoDD v. 2 (Figure 14). Cooler colors represent earlier activity and warmer colors represent the later stages of the swarm.

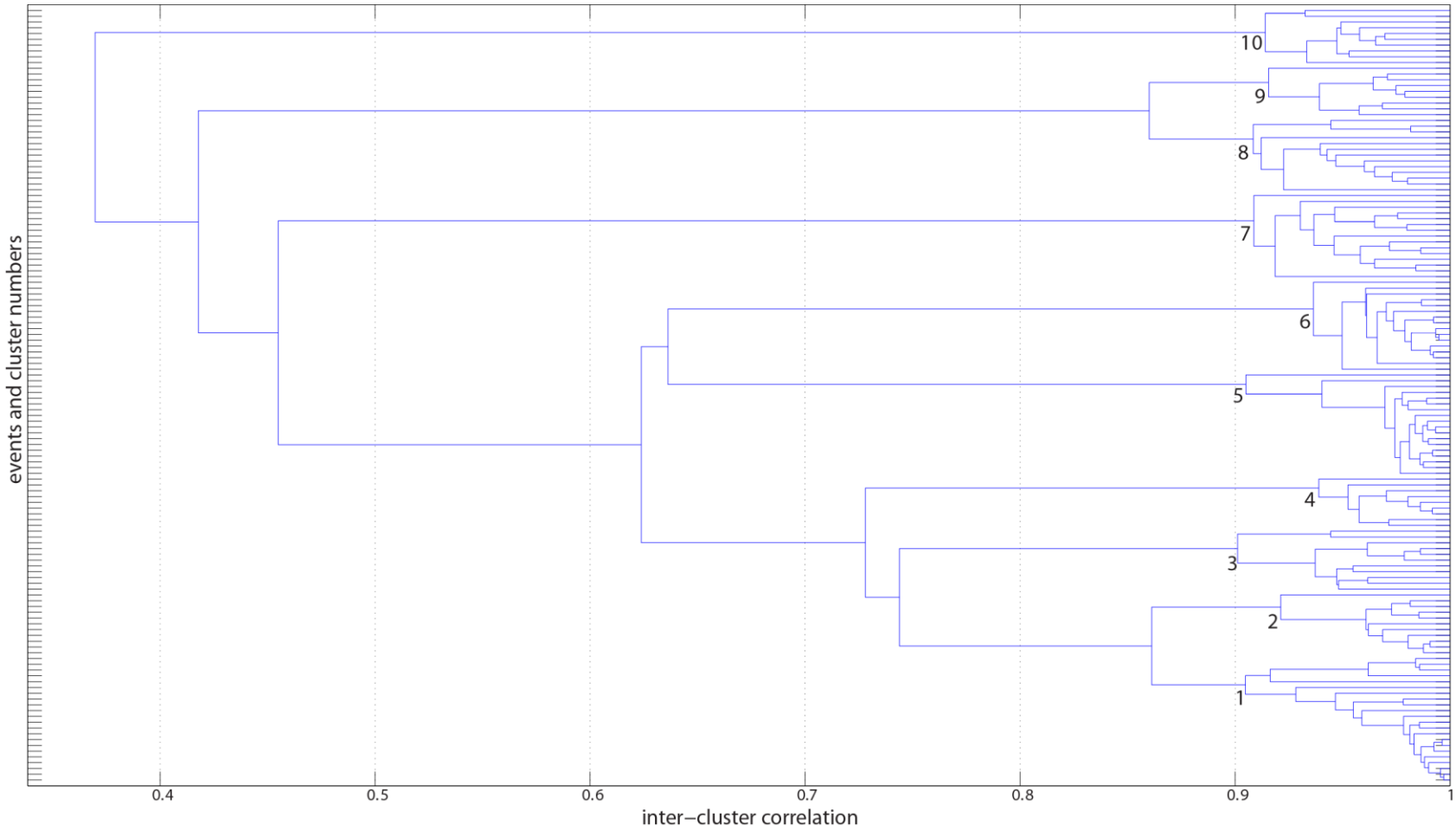

Figure 16. Events can be broken down into clusters with similar waveforms known as multiplets. This dendrogram shows the events from the ten largest clusters with a correlation coefficient of 0.9 and how they relate to one another. The root of each cluster is labeled with its corresponding number.

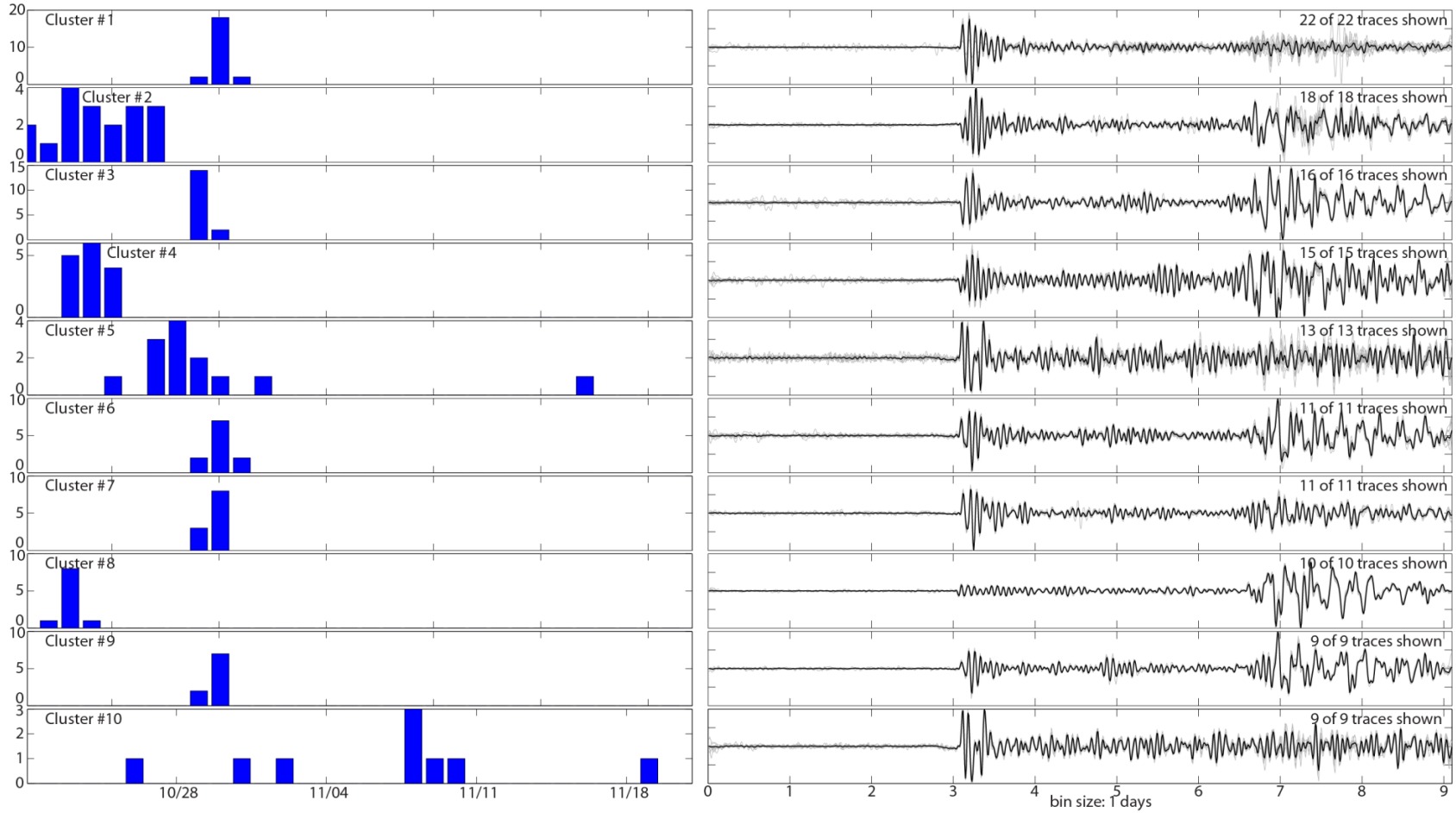

Figure 17. Multiplets with a correlation-coefficient of 0.9. The occurrence histograms (left) show the number of well-correlated events and the days that they occurred on. The waveform traces (right) show the stacked events in bold for each multiplet cluster and the traces of each event in light grey.

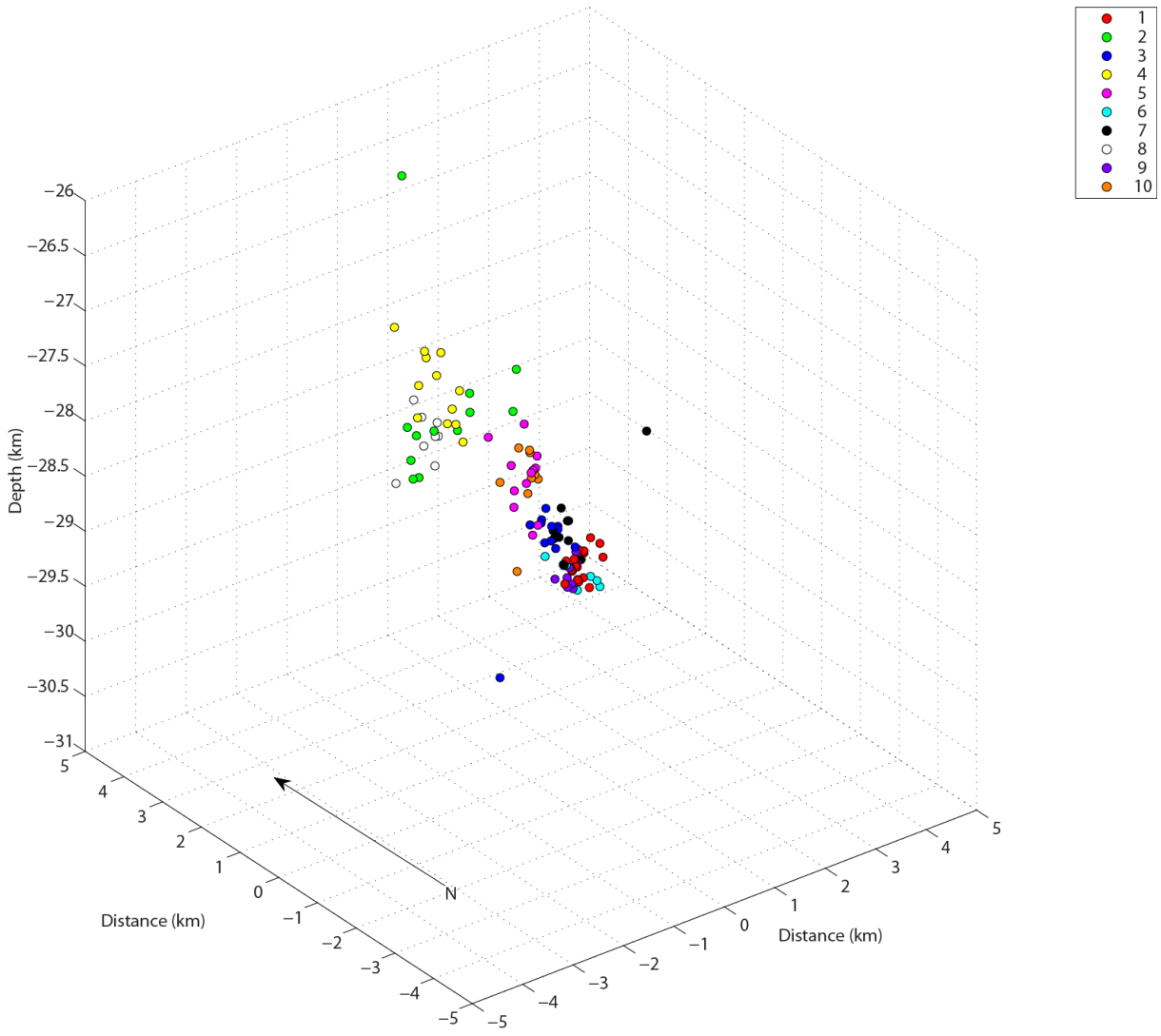

Figure 18. Locations of the event multiplets with minimum cross-correlations of 0.9. The legend shows the cluster number, which corresponds with the clusters shown in Figure 17.

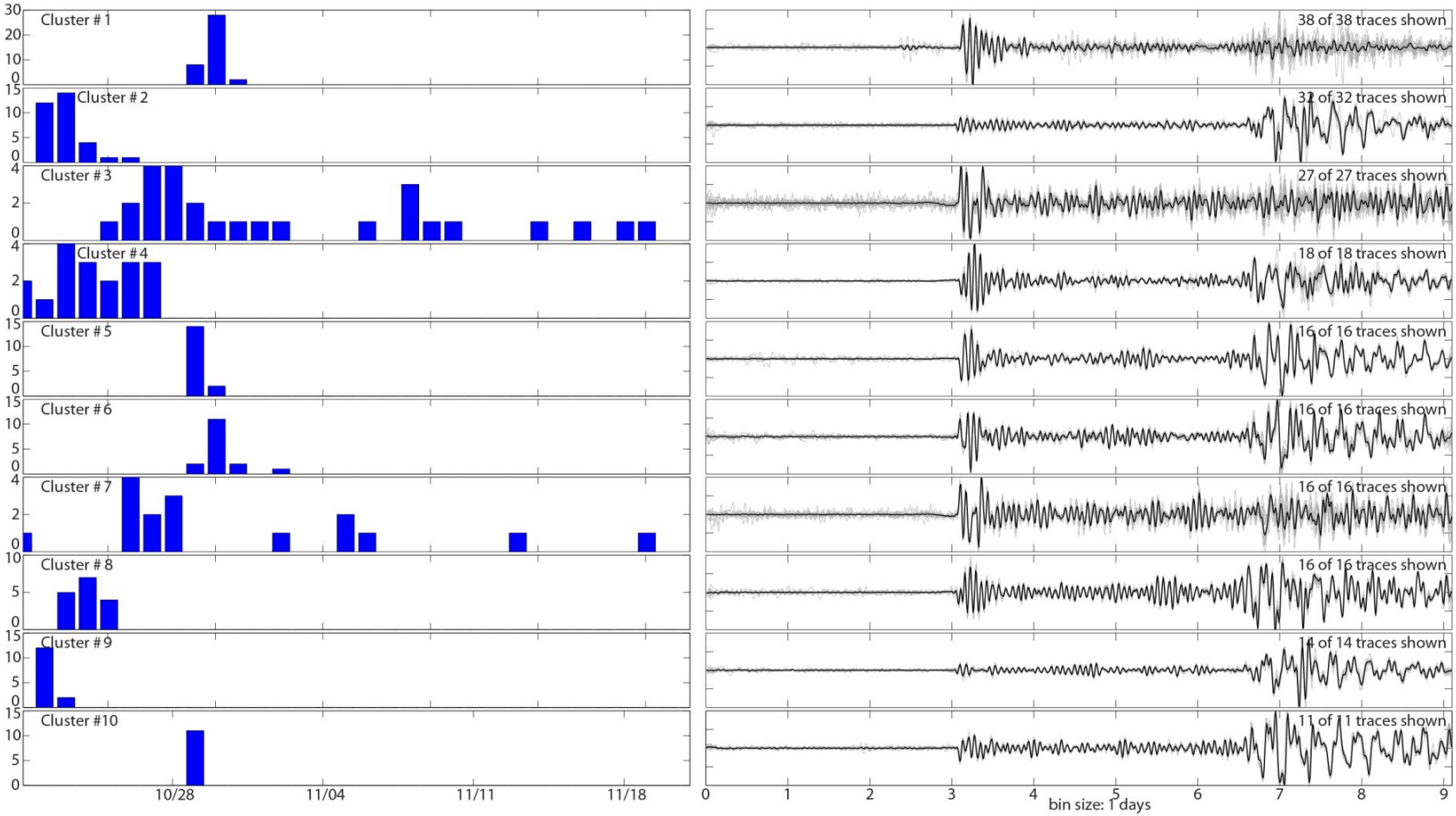

Figure 19. Multiplets with a correlation-coefficient of 0.8. The occurrence histograms (left) show the number of well-correlated events within each multiplet and the days that they occurred on. The waveform traces (right) show the stacked events in bold for each multiplet cluster and the traces of each event in light grey.

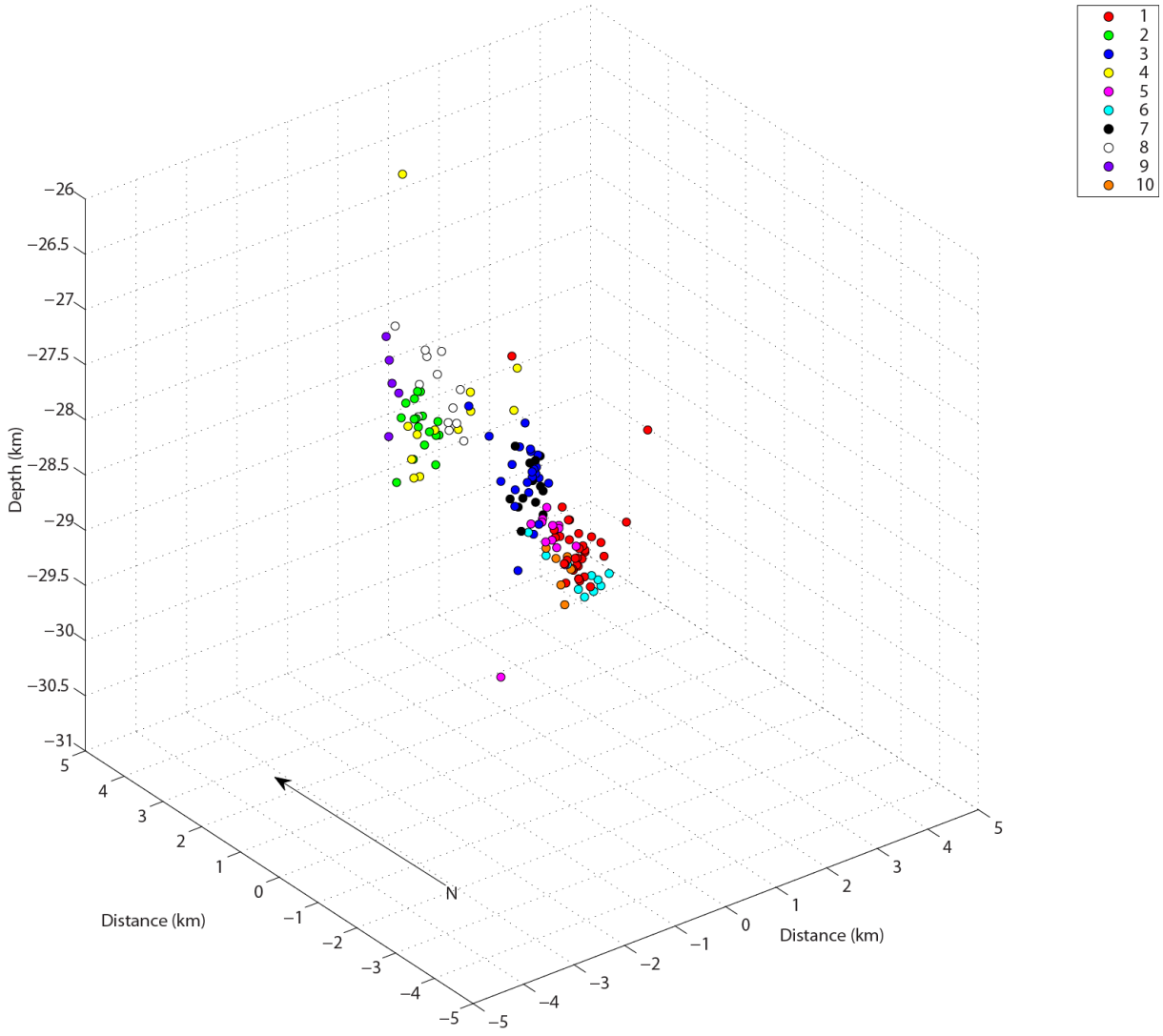

Figure 20. Locations of the event multiplets with minimum cross-correlations of 0.8. The legend shows the cluster number, which corresponds with the multiplet clusters shown in Figure 19.

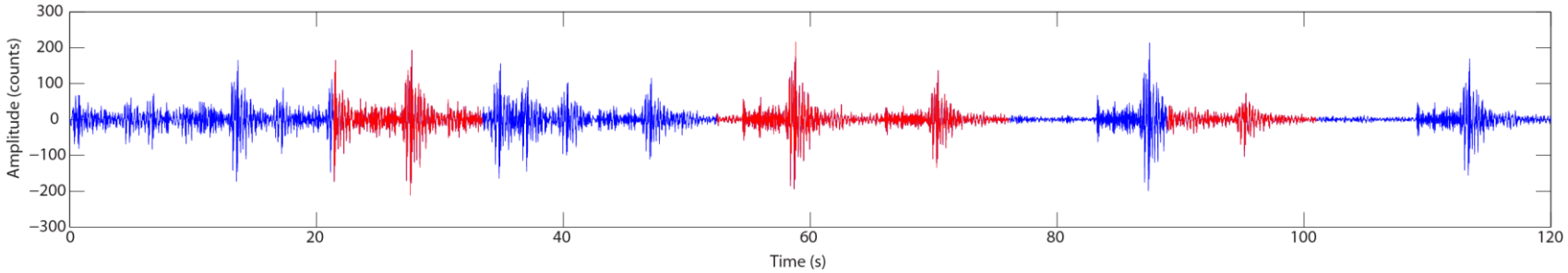

Figure 21. Waveforms from a spasmodic burst sequence at station NZ02 that occurred on Oct. 22nd from 8:46 to 8:48 UTC. The events highlighted in red have a minimum correlation of 70% with a reference event that occurred at 8:44:15 UTC. Because many of the waveforms overlap they are difficult to distinguish from one another and finding their absolute locations by phase-picking is very difficult and inaccurate.

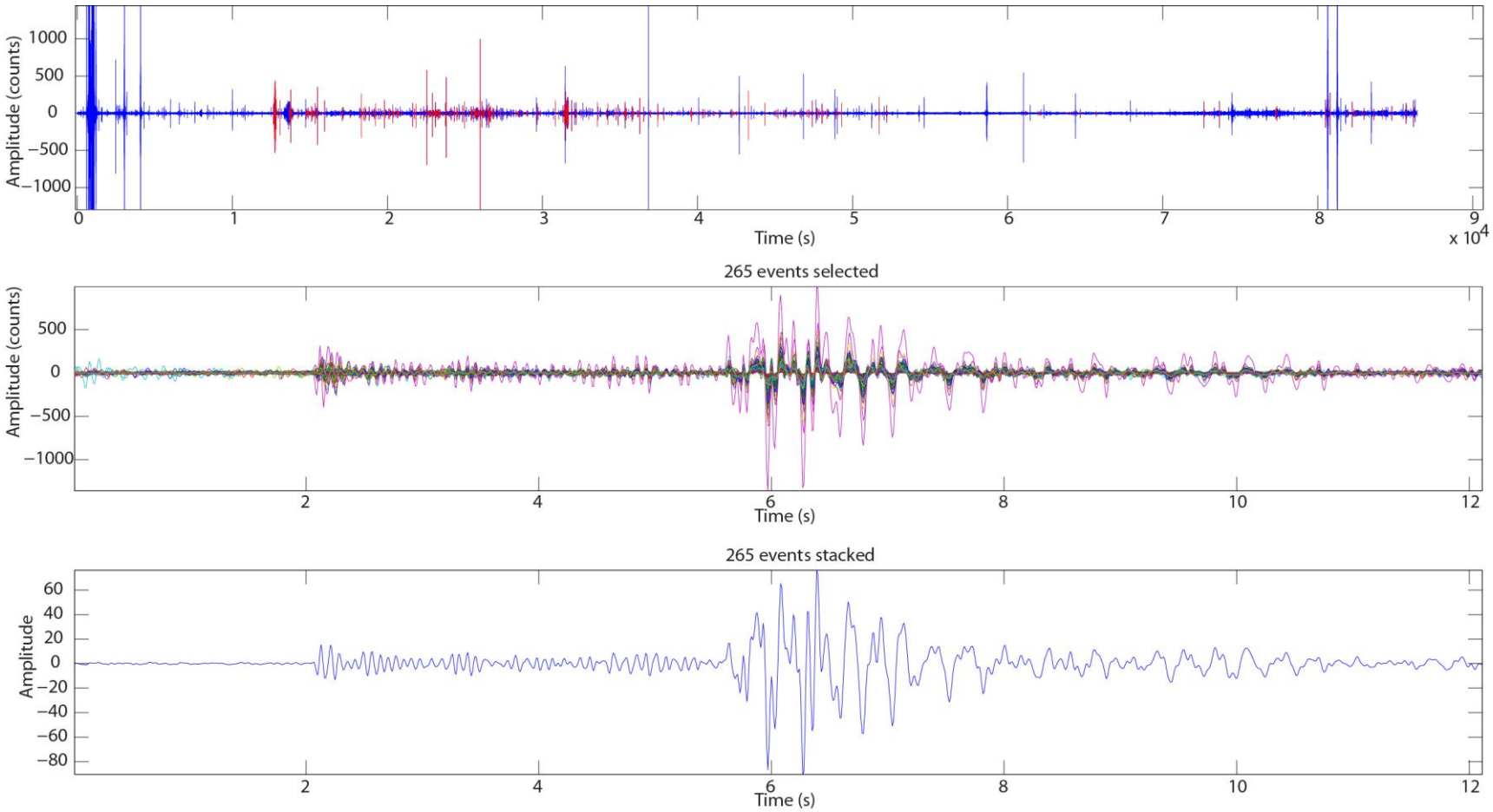

Figure 22. Spasmodic burst events from Oct. 22nd, 2009. The top graph shows waveform data from NZ02 for the entire day with well-correlated (70%) events highlighted in red. The middle graph shows the waveform traces of each event overlaid. The bottom graph shows the stacked waveform of all 265 events.

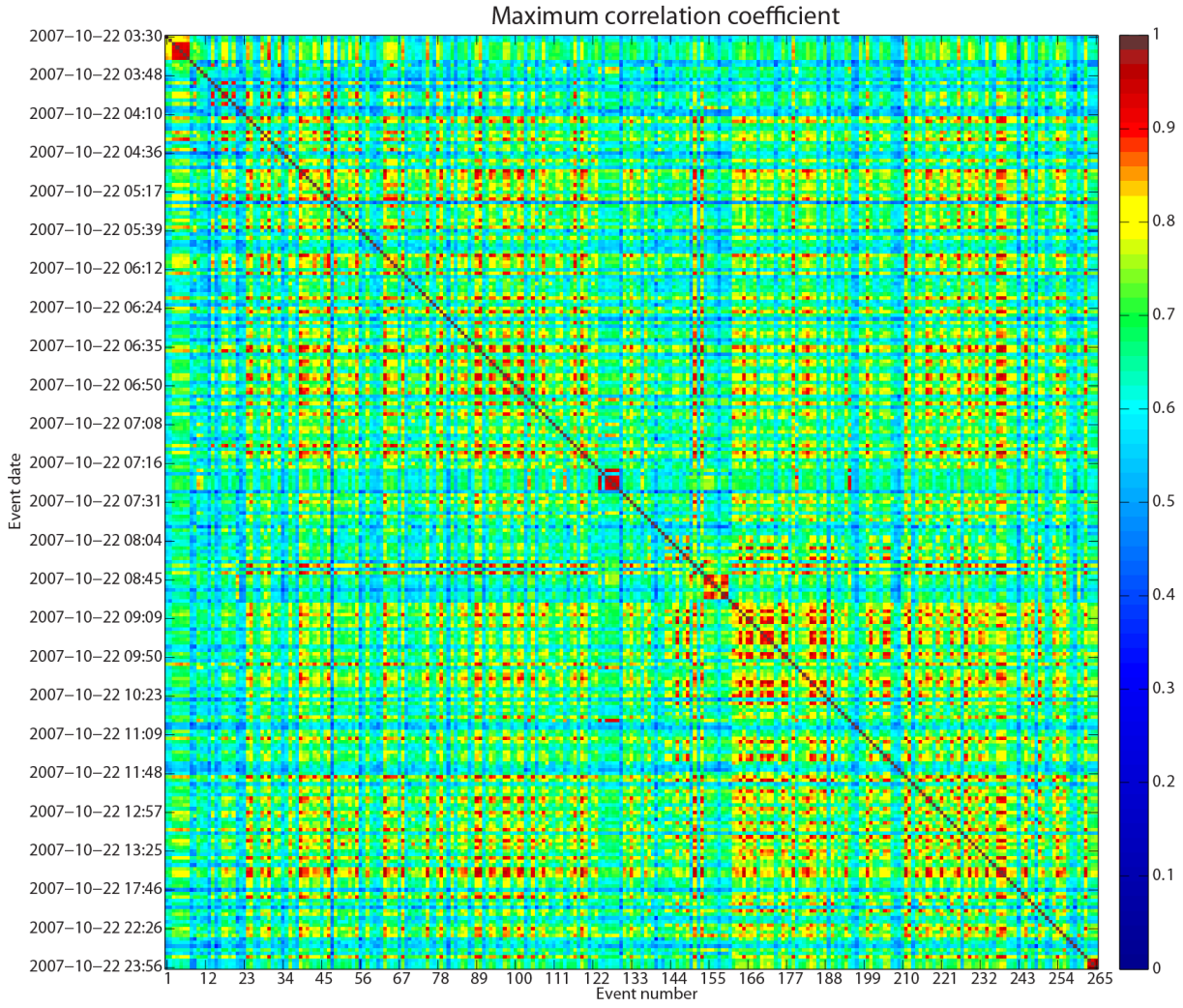

Figure 23. Cross-correlation matrix of the 265 events from the Oct. 22nd spasmodic bursts at station NZ02. Cooler colors are the least well-correlated events and warmer colors are the most well-correlated events. Events are organized and numbered by the date of their occurrence; therefore the earliest events have the lowest numbers. The diagonal line running from the upper-left to the lower-right hand corners are events compared with themselves (auto-correlation); note that they have a correlation of 1.0.

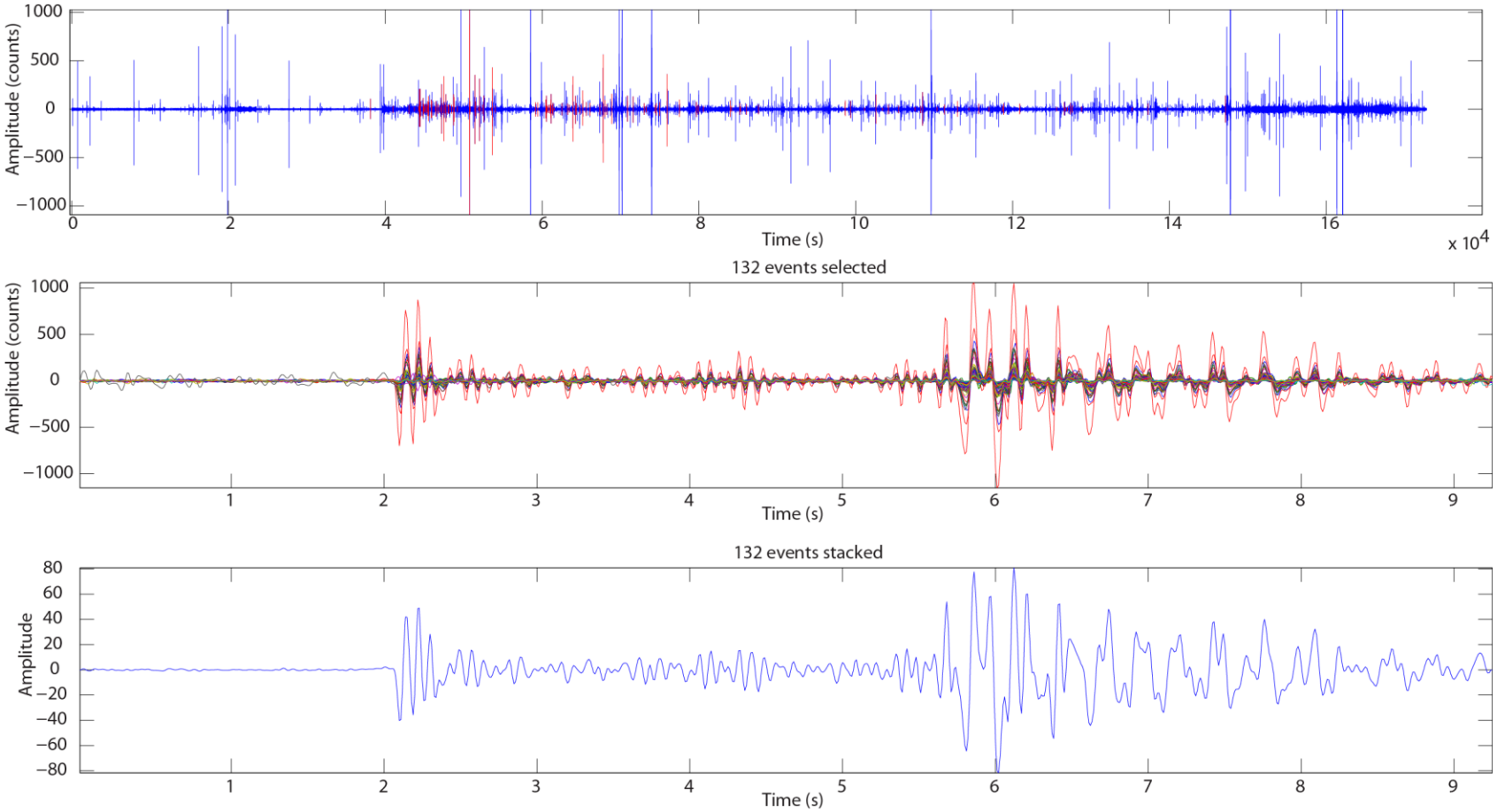

Figure 24. Spasmodic burst events from Oct. 29th-30th, 2009. The top graph shows waveform data from NZ02 for the entire day with well-correlated (70%) events highlighted in red. The middle graph shows the waveform traces of each event overlaid. The third graph shows the stacked waveform of all 132 events.

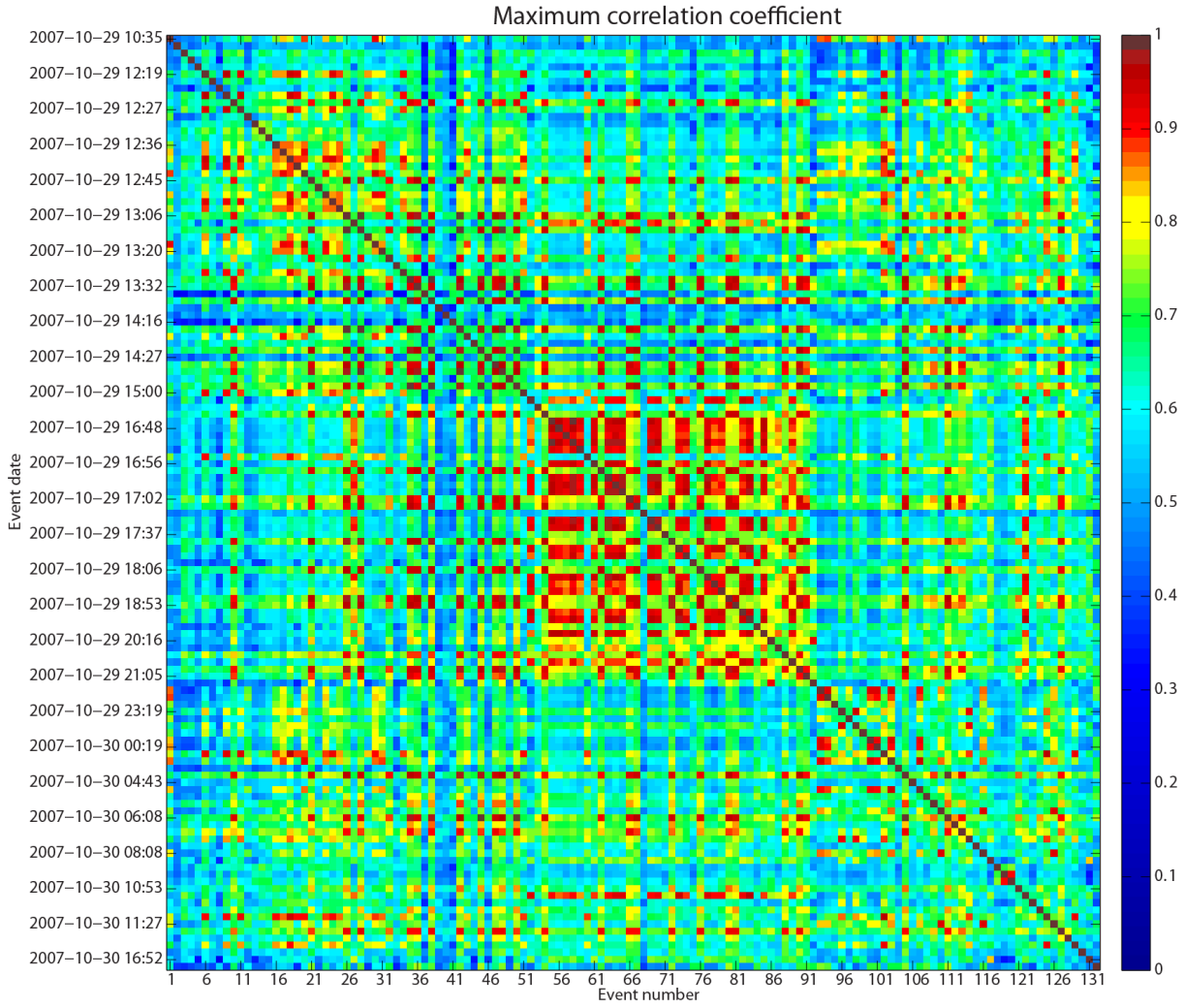

Figure 25. Cross-correlation matrix of the 132 events from the Oct. 29th-30th spasmodic bursts at station NZ02. Cooler colors are the least well-correlated events and warmer colors are the most well-correlated events. Events are organized and numbered by the date of their occurrence; therefore the earliest events have the lowest numbers. The diagonal line running from the upper-left to the lower-right hand corners are events compared with themselves (auto-correlation); note that they have a correlation of 1.0.

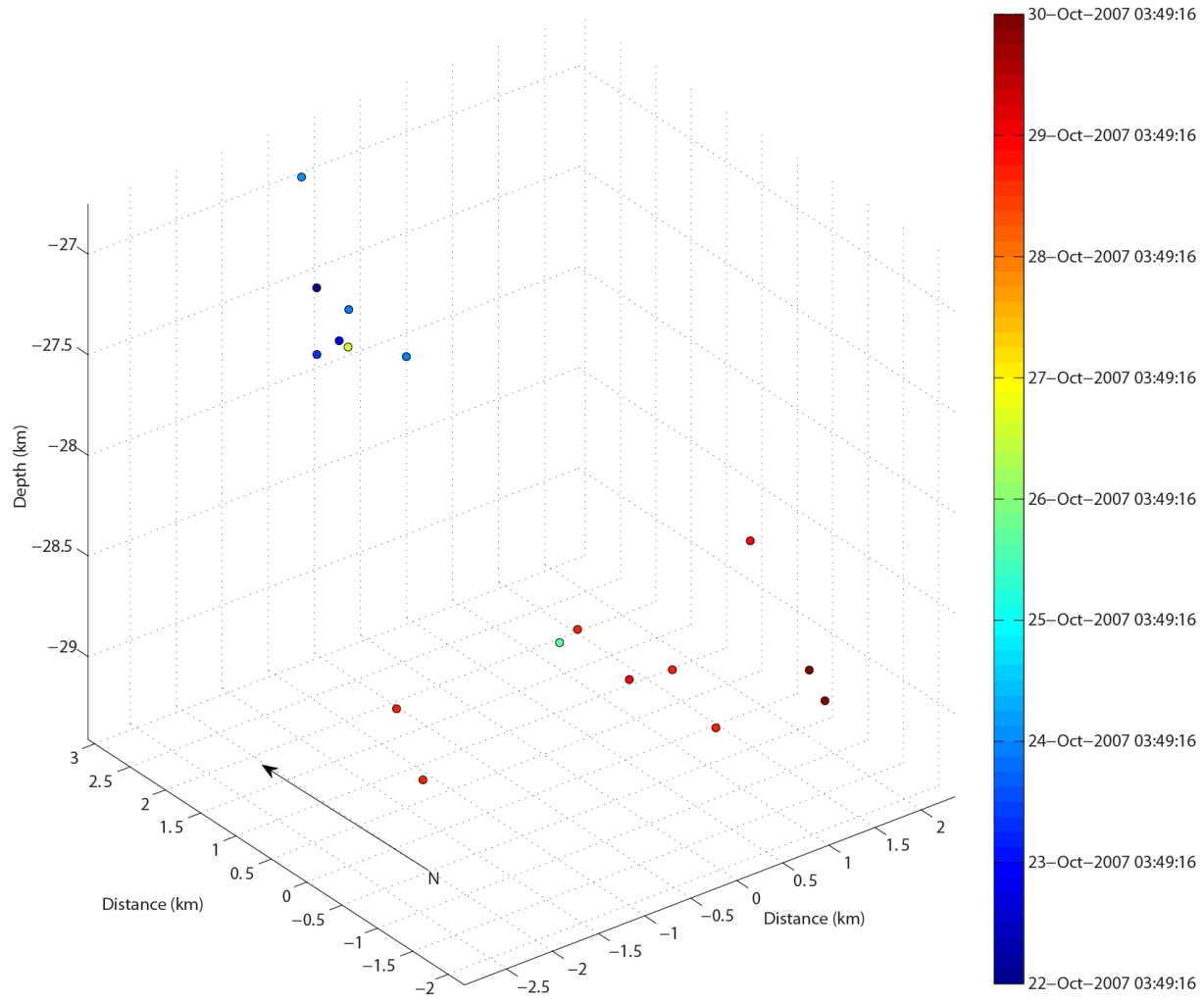

Figure 26. Time series plot of selected events from spasmodic bursts. The locations are derived from the HypoDD v. 2 data. Cooler colors represent earlier activity and warmer colors represent the later stages of the swarm.

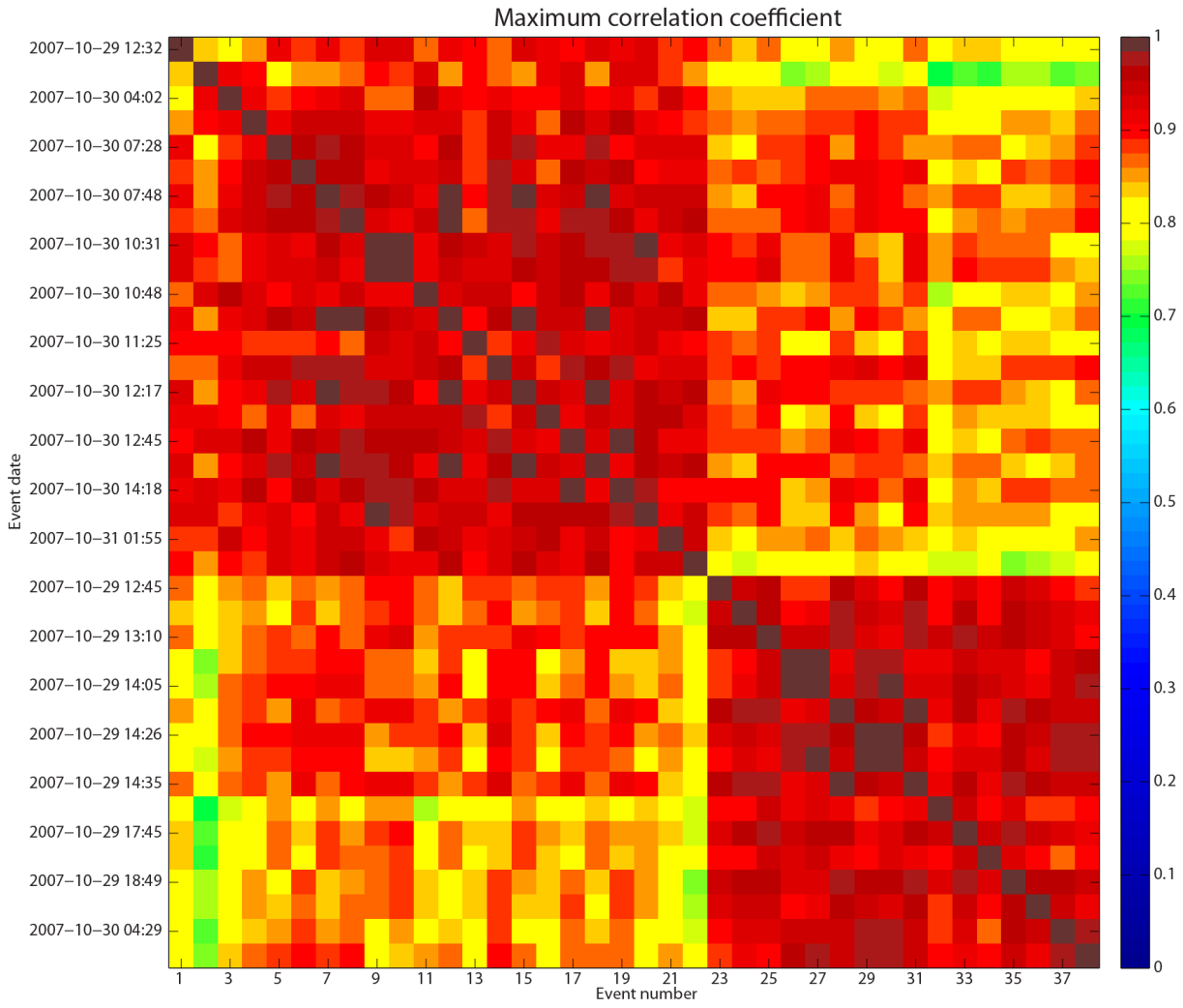

Figure 27. Cross-correlation matrix comparing p-waves at station NZ02 from cluster 1 (events 1-22) to the p-waves from cluster 3 (events 23-38) (Figure 17), after they have been inverted, when using a correlation coefficient of 0.9. Cooler colors are the least well-correlated events and warmer colors are the most well-correlated events. Events are organized and numbered by the date of their occurrence; therefore the earliest events have the lowest numbers. The diagonal line running from the upper-left to the lower-right hand corners are events compared with themselves (auto-correlation); note that they have a correlation of 1.0.

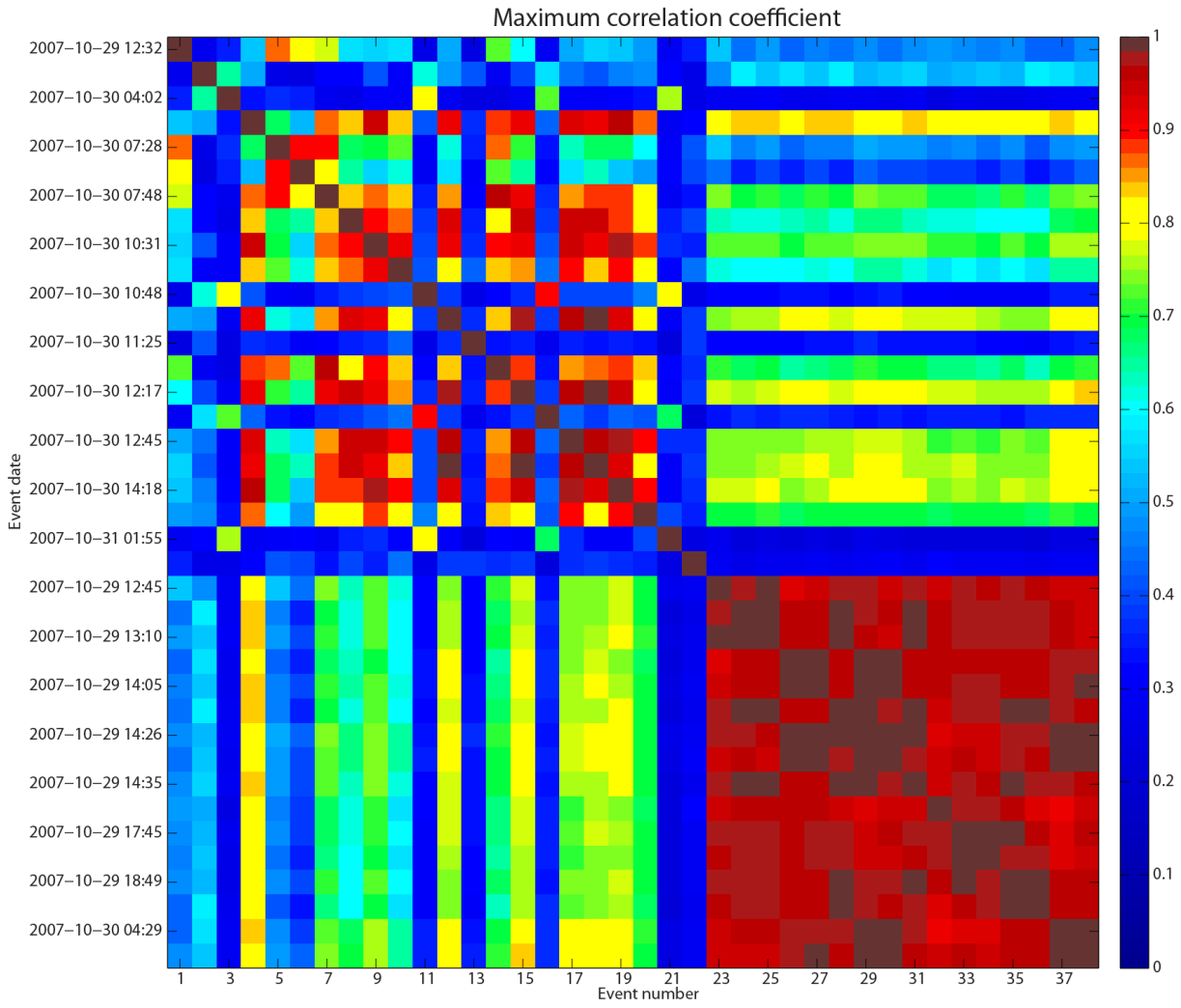

Figure 28. Cross-correlation matrix comparing s-waves at station NZ02 from cluster 1 (events 1-22) to the s-waves from cluster 3 (events 23-38) (Figure 17), after they have been inverted, when using a correlation coefficient of 0.9. Cooler colors are the least well-correlated events and warmer colors are the most well-correlated events. Events are organized and numbered by the date of their occurrence; therefore the earliest events have the lowest numbers. The diagonal line running from the upper-left to the lower-right hand corners are events compared with themselves (auto-correlation); note that they have a correlation of 1.0.

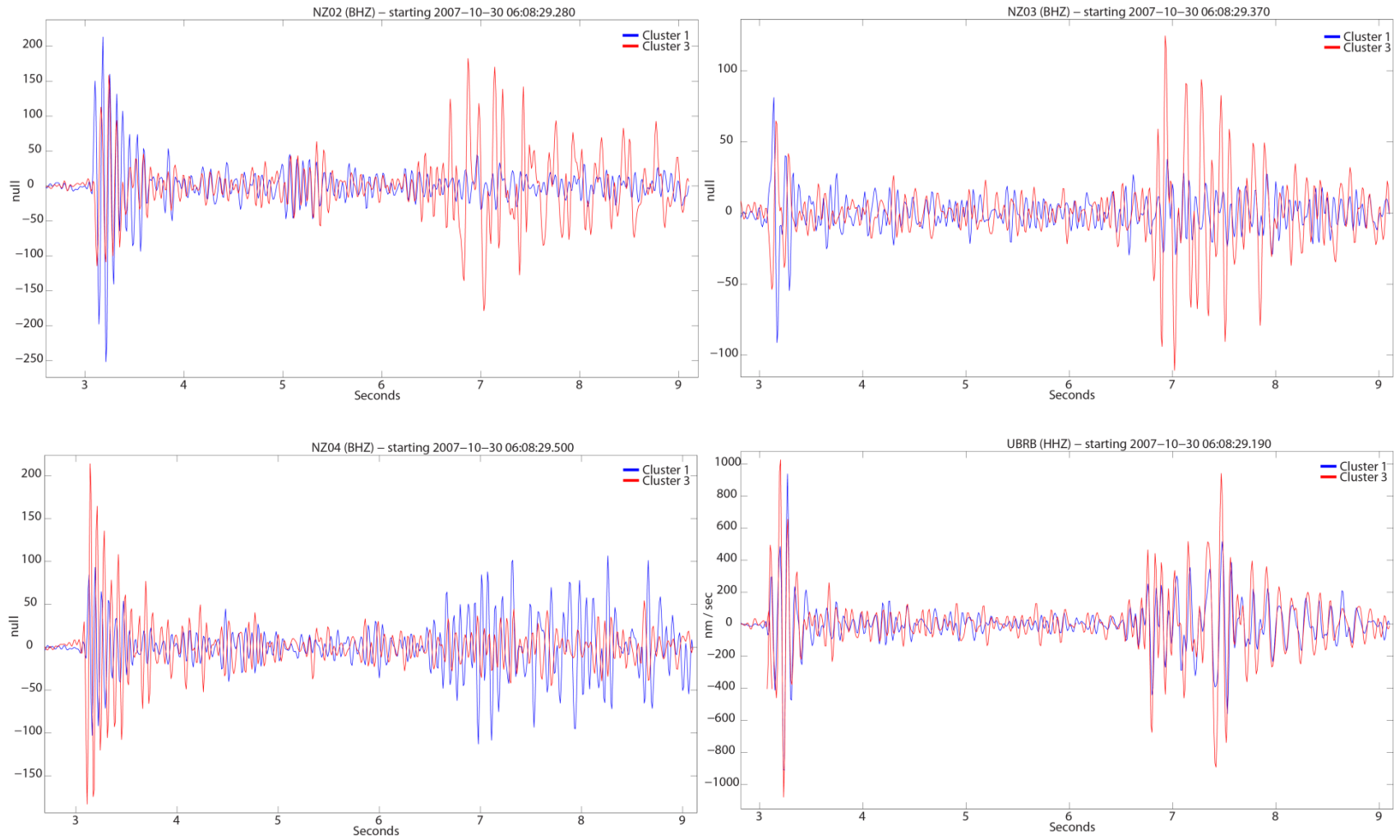

Figure 29. Overlain stacked waveforms for clusters 1 (blue) and 3 (red), showing inverted P-waves at stations NZ02 (upper left), NZ03 (upper right), NZ04 (lower left), and UBRB (lower right).

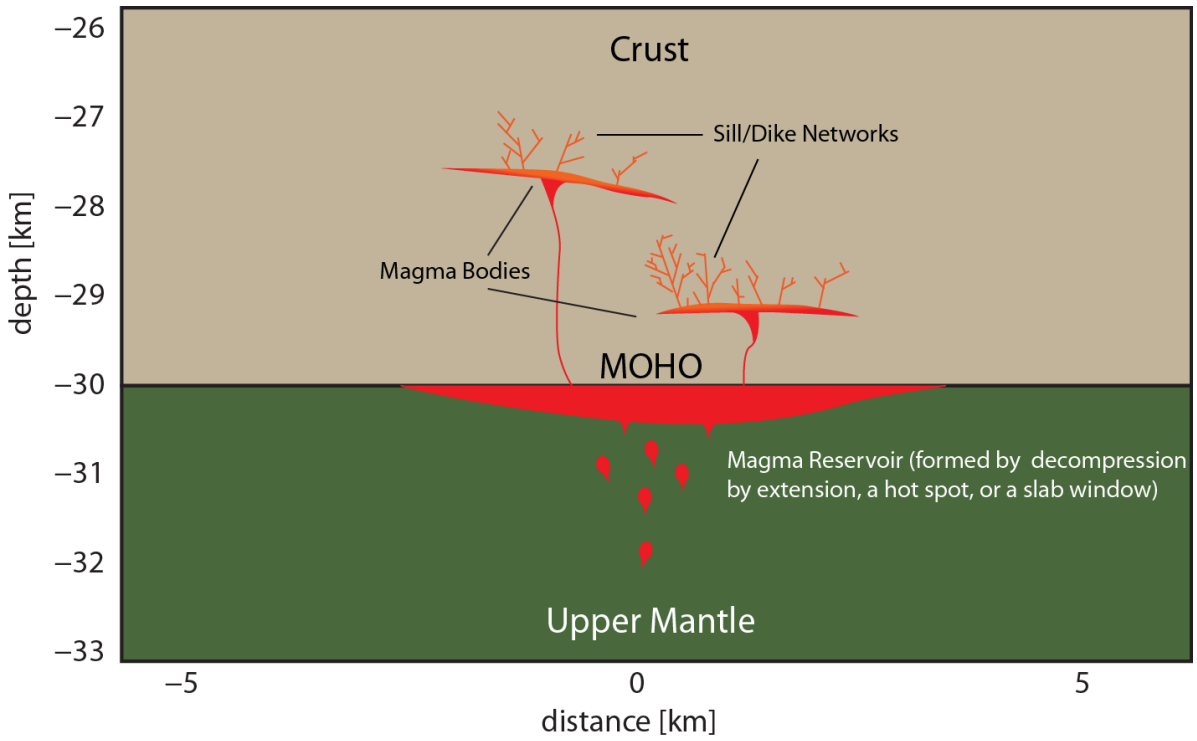

Figure 30. Illustration of the proposed source for seismic unrest during the Nechako swarm. The existence of two magma bodies have been hypothesized, based on two spatially and temporally distinct phases of seismic activity, as part of a complex network developed from underplating. The buoyant rise of magma, resulting from crystal fractionation within the magma bodies, or a new injection of magma from a mantle source, causing the surrounding crust to fracture, are possible causes of the swarm. Earthquake multiplets that occurred within a short time of one another are thought to be the result of propagating fractures within dikes and/or sills due to the migration of magma. Several sources have been suggested for causing past volcanic features, including decompression by extension (Bevier, 1983a; Edwards and Russell, 1999), a hot spot (Bevier, 1979; Mercier et al., 2009), or a slab window (Thorkelson and Taylor, 1989; Thorkelson et al., 2011).

Works Cited

Bevier, M.L., 1989, A lead and strontium isotopic study of the Anahim volcanic belt, British Columbia: Additional evidence for widespread suboceanic mantle beneath western North America: Bulletin of the Geological Society of America, v. 101, no. 7, p. 973.

Bevier, M.L., 1983a, Implications of chemical and isotopic composition for petrogenesis of Chilcotin Group basalts, British Columbia: Journal of Petrology, v. 24, no. 2, p. 207–226.

Bevier, M.L., 1983b, Regional stratigraphy and age of Chilcotin Group basalts, south-central British Columbia: Canadian Journal of Earth Sciences, v. 20, p. 515–524.

Bevier, M.L., Armstrong, R.L., and Souther, J.G., 1979, Miocene peralkaline volcanism in west-central British Columbia–Its temporal and plate-tectonics setting: Geology, v. 7, no. 8, p. 389.

Cassidy, J.F., Balfour, N., Hickson, C., Kao, H., White, R., Caplan-Auerbach, J., Mazzotti, S., Rogers, G.C., Al-Khoubbi, I., Bird, A.L., Esteban, L., Kelman, M., Hutchinson, J., and McCormack, D., 2011, The 2007 Nazko, British Columbia, Earthquake Sequence: Injection of Magma Deep in the Crust beneath the Anahim Volcanic Belt: Bulletin of the Seismological Society of America, v. 101, no. 4, p. 1732–1741.

Chouet, B.A., Page, R.A., Stephens, C.D., Lahr, J.C., and Power, J.A., 1994, Precursory swarms of long-period events at Redoubt Volcano (1989-1990), Alaska: Their origin and use as a forecasting tool: Journal of volcanology and geothermal research, v. 62, no. 1-4, p. 95–135.

Cox, K.G., 1980, A model for flood basalt vulcanism: Journal of Petrology, v. 21, no. 4, p. 629–650.

Cox, A., and Engebretson, D.C., 1985, Change in motion of Pacific plate at 5 Myr BP: Nature, v. 313, no. 6002, p. 472–474.

Doubrovine, P.V., and Tarduno, J.A., 2008, A revised kinematic model for the relative motion between Pacific oceanic plates and North America since the Late Cretaceous: Journal of geophysical research, v. 113, no. B12, p. B12101.

Edwards, B.R., and Russell, J.K., 1999, Northern Cordilleran volcanic province: A northern Basin and Range?: Geology, v. 27, no. 3, p. 243 –246.

La Femina, P.C., Connor, C.B., Hill, B.E., Strauch, W., and Saballos, J.A., 2004, Magma-tectonic interactions in Nicaragua: the 1999 seismic swarm and eruption of Cerro Negro volcano: Journal of Volcanology and Geothermal Research, v. 137, no. 1-3, p. 187–199.

Furlong, K.P., and Fountain, D.M., 1986, Continental crustal underplating: thermal considerations and seismic-petrologic consequences: Journal of Geophysical Research, v. 91, no. B8, p. PP. 8285–8294.

Gutenberg, B., and Richter, C.F., 1944, Frequency of earthquakes in California: Bulletin of the Seismological Society of America, v. 34, no. 4, p. 185–188.

Hill, D.P., Dawson, P., Johnston, M.J.S., Pitt, A., Biasi, G., and Smith, K., 2002, Very-long-period volcanic earthquakes beneath Mammoth Mountain, California:.

Hill, D.P., Ellsworth, W.L., Johnston, M.J.S., Langbein, J.O., Oppenheimer, D.H., Pitt, A.M., Reasenberg, P.A., Sorey, M.L., and McNutt, S.R., 1990, The 1989 earthquake swarm beneath Mammoth Mountain, California: An initial look at the 4 May through 30 September activity: Bulletin of the Seismological Society of America, v. 80, no. 2, p. 325.

Hutchinson, J.A., and Caplan-Auerbach, J., 2010, New perspectives on the 2007 seismic swarm in the Anahim Volcanic Belt, British Columbia, from earthquake cross-correlation and high-resolution relocations, *in* AGU Fall Meeting Abstracts, p. 2039.

Ishimoto, M., and Iida, K., 1939, Observations of earthquakes registered with the microseismograph constructed recently: Bull. Earthq. Res. Inst, v. 17, p. 443–478.

Jarchow, C.M., Thompson, G.A., Catchings, R.D., and Mooney, W.D., 1993, Seismic evidence for active magmatic underplating beneath the Basin and Range province, western United States: Journal of geophysical research, v. 98, no. B12, p. 22095–22.

Lahr, J.C., Chouet, B.A., Stephens, C.D., Power, J.A., and Page, R.A., 1994, Earthquake classification, location, and error analysis in a volcanic environment: implications for the magmatic system of the 1989-1990 eruptions at Redoubt Volcano, Alaska: Journal of Volcanology and Geothermal Research, v. 62, no. 1-4, p. 137–151.

McNutt, S.R., 1992, Volcanic tremor, *in* Encyclopedia of earth system science, Academic Press, San Diego, p. 417–425.

Mercier, J.P., Bostock, M.G., Cassidy, J.F., Dueker, K., Gaherty, J.B., Garnero, E.J., Revenaugh, J., and Zandt, G., 2009, Body-wave tomography of western Canada: Tectonophysics, v. 475, no. 3-4, p. 480–492.

Minakami, T., 1974, Seismology of volcanoes in Japan, *in* Civetta, L., Gasparini, P., Luongo, G., and Rapolla, A. eds., Physical Volcanology, Elsevier, Amsterdam, p. 1–27.

Mogi, K., 1962, Study of elastic shocks caused by the fracture of heterogeneous materials and its relations to earthquake phenomena: Bulletin of the Earthquake Research Institute, v. 40, p. 125–173.

Pollitz, F.F., 1988, Episodic North America and Pacific Plate motions: Tectonics, v. 7, no. 4, p. PP. 711–726.

Reyes, C.G., and West, M.E., 2011, The Waveform Suite: A robust platform for manipulating waveforms in MATLAB: Seismological Research Letters, v. 82, no. 1, p. 104.

Roman, D.C., De Angelis, S., Latchman, J.L., and White, R., 2008, Patterns of volcanotectonic seismicity and stress during the ongoing eruption of the Soufrière Hills Volcano, Montserrat (1995-2007): Journal of Volcanology and Geothermal Research, v. 173, no. 3-4, p. 230–244.

Rubin, A.M., 1993, Tensile fracture of rock at high confining pressure: implications for dike propagation: Journal of Geophysical Research, v. 98, no. B9, p. 15919–15.

Rubin, A.M., Gillard, D., and Got, J.L., 1998, A reinterpretation of seismicity associated with the January 1983 dike intrusion at Kilauea Volcano, Hawaii: Journal of geophysical research, v. 103, no. B5, p. 10003–10015.

Sherburn, S., Scott, B.J., Nishi, Y., and Sugihara, M., 1998, Seismicity at White Island volcano, New Zealand: a revised classification and inferences about source mechanism: Journal of Volcanology and Geothermal Research, v. 83, no. 3-4, p. 287–312.

Smith, K.D., von Seggern, D., Blewitt, G., Preston, L., Anderson, J.G., Wernicke, B.P., and Davis, J.L., 2004, Evidence for deep magma injection beneath Lake Tahoe, Nevada-California: Science, v. 305, no. 5688, p. 1277.

Souther, J.G., Clague, J.J., and Mathewes, R.W., 1987, Nazko cone: a Quaternary volcano in the eastern Anahim Belt: Canadian Journal of Earth Sciences, v. 24, no. 12, p. 2477–2485.

Stacey, R.A., 1974, Plate tectonics, volcanism and the lithosphere in British Columbia: Nature, v. 250, no. 5462, p. 133–134.

Thorkelson, D.J., Madsen, J.K., and Sluggett, C.L., 2011, Mantle flow through the Northern Cordilleran slab window revealed by volcanic geochemistry: Geology, v. 39, no. 3, p. 267 –270.

Thorkelson, D.J., and Taylor, R.P., 1989, Cordilleran slab windows: Geology, v. 17, no. 9, p. 833.

Waldhauser, F., 2001, HypoDD-A program to compute double-difference hypocenter locations: US Geological Survey. Open File Report,, p. 01–113.

Waldhauser, F., and Ellsworth, W.L., 2000, A double-difference earthquake location algorithm: method and application to the northern Hayward fault, California: Bulletin of the Seismological Society of America, v. 90, no. 6, p. 1353–1368.

Weinberger, R., Lyakhovsky, V., Baer, G., and Agnon, A., 2000, Damage zones around en echelon dike segments in porous sandstone: J. geophys. Res, v. 105, p. 3115–3133.

White, R.S., Drew, J., Martens, H.R., Key, J., Soosalu, H., and Jakobsdóttir, S.S., 2011, Dynamics of dyke intrusion in the mid-crust of Iceland: Earth and Planetary Science Letters, v. 304, p. 300–312.

Wyss, M., 1973, Towards a physical understanding of the earthquake frequency distribution: Geophysical Journal of the Royal Astronomical Society, v. 31, no. 4, p. 341–359.

Zhang, H., and Thurber, C.H., 2003, Double-difference tomography: The tethod and its application to the Hayward Fault, California: Bulletin of the Seismological Society of America, v. 93, no. 5, p. 1875 –1889.

Appendices

Included in these appendices are descriptions for the input and output files used for various programs as well as Matlab scripts written for analysis and generating figures. The files are included on a CD supplement. Additional figures are included in Appendix 4.

Appendix 1 – Program Input Files

HypoDD

- event.dat – absolute locations calculated with the Antelope program dbloc2. Used as an input file for HypoDD.
- ph2dt.inp – input parameters for ph2dt, which was used to generate the catalogue of travel time differences for the absolute locations.
- dt.ct – catalog of travel time differences for pairs of events.
- sta.dat – station location and elevation information.
- hypoDD07_2d.inp, hypoDD08_2d.inp, hypoDD09_2d.inp – input parameters for HypoDD v. 1, using a 1-dimensonal velocity model and cross correlation catalogs with coefficients of 0.7, 0.8, and 0.9.
- hypoDD07long.inp, hypoDD08long.inp, hypoDD09long.inp – input parameters for HypoDD v. 2, using a 3-dimensional velocity model and cross correlation catalogs with coefficients of 0.7, 0.8, and 0.9.
- hypoDD06long_svd1.inp, hypoDD07long_svd1.inp, hypoDD08long_svd1.inp, hypoDD09long_svd1.inp – input parameters for HypoDD v. 2, using a 3-dimensional velocity model and cross correlation catalogs with coefficients of 0.6, 0.7, 0.8, and 0.9. These parameters were used specifically to calculate the uncertainty for a subset of events using the singlular value decomposition (SVD) double-difference relocation algorithm.
- vel3d.vel – revised velocity model generated by TomoDD and used as an input for HypoDD v. 2. Edited to be compatible with HypoDD v. 2.

TomoDD

- MOD – 3-dimensional velocity derived from the 1-dimensional velocity model by Cassidy et al. (2011).
- tomosta.dat – station location and elevation information.
- absolute.dat – absolute location data derived from the dbloc2 data set.

- tomdd07long.inp, tomodd08long.inp, tomodd09long.inp – input parameters for TomoDD , using a 3-dimensional velocity model derived from Cassidy et al. (2011) and cross correlation catalogs with coefficients of 0.7, 0.8, and 0.9.

Cross Correlation

- matddlong_scp07, matddlong_scp08, matddlong_scp09 – input parameters to cross correlate phases for pairs of events using correlation coefficients of 0.7, 0.8, and 0.9.

Appendix 2 – Program Output Files

HypoDD

- hypoDD07_2d.reloc, hypoDD08_2d.reloc, hypoDD09_2d.reloc – event relocations calculated with HypoDD v. 1, using a 1-dimensonal velocity model and cross correlation catalogs with coefficients of 0.7, 0.8, and 0.9.
- hypoDD07long.reloc, hypoDD08long.reloc, hypoDD09long.reloc – event relocations calculated with HypoDD v. 2, using a 3-dimensional velocity model and cross correlation catalogs with coefficients of 0.7, 0.8, and 0.9.
- hypoDD06long_svd1.reloc, hypoDD07long_svd1.reloc, hypoDD08long_svd1.reloc, hypoDD09long_svd1.reloc – event relocations calculated with HypoDD v. 2, using a 3-dimensional velocity model and cross correlation catalogs with coefficients of 0.6, 0.7, 0.8, and 0.9. These parameters were used specifically to calculate the uncertainty for a subset of events using the singlular value decomposition (SVD) double-difference relocation algorithm.

TomoDD

- tomdd07long.reloc, tomodd08long.reloc, tomodd09long.reloc – event relocations calculated with TomoDD , using a 3-dimensional velocity model derived from Cassidy et al. (2011) and cross correlation catalogs with coefficients of 0.7, 0.8, and 0.9.
- Vp_model09long.dat, Vs_model09long.dat – revised P and S phase velocity models, derived from Cassidy et al. (2011). Also, after editing, used for the velocity model input for HypoDD v. 2.

Cross Correlation

- dtlong07.cc, dtlong08.cc, dtlong09.cc – catalog of differential travel times generated by cross-correlating pairs of events with coefficients of 0.7, 0.8, and 0.9.

Appendix 3 – Matlab Scripts

- clusterplot.m – used to cluster multiplets and plot them on a 3-dimensional plot.
- cross.m – generates vertical cross-sectional plots of a 3-dimensional velocity model. Modified from the original by Jeremy Pesicek.
- eqcompare.m – plots all of the events from a location or relocation file side-by-side with events from a different file for comparison. Modified from eqplot.m from the GISMO suite.
- findorid.m – creates a waveform correlation object out of specific events based on their origin id numbers. This was used to plot events from the spasmodic bursts.
- horiz.m - generates horizontal cross-sectional plots of a 3-dimensional velocity model. Modified from the original by Jeremy Pesicek.
- Jfiltfilt.m – filters waveform data. Created by Jackie Caplan-Auerbach.
- nazkolope.m – converts waveform data from an Antelope database into a correlation object, based on a reference event, over a specified period of time
- plot3d.m – creates a 3-dimensional plot using event locations.
- spasplot.m – used to plot events found with findorid.m.
- sta_lta.m – identifies events over a specified period of time by comparing waveform amplitudes during a short term average over a long term average. Created by Jackie Caplan-Auerbach.
- sta_ltaprep - used to input waveforms from an Antelope database into the script sta_lta.m.

Appendix 4 – Additional Figures

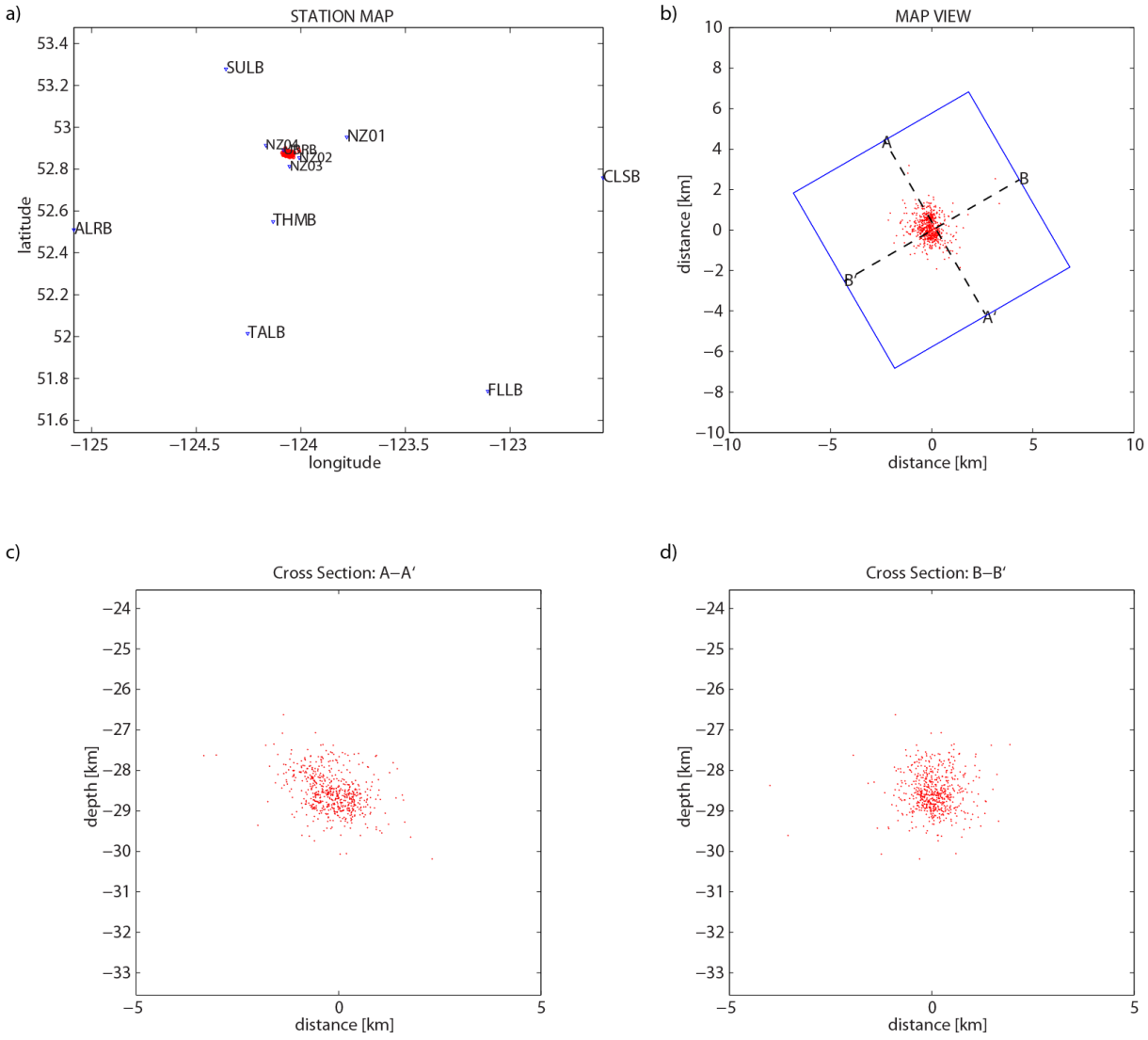

Figure A - 1. a) Epicentral relocations relative to the POLARIS and temporary stations. Relocations were calculated using HypoDD v. 1 and a catalog of cross-correlations with a coefficient of 0.8. b) Close-up view of epicenters. The section lines show the orientation of the cross sections in figures A-1c and A-1d below, which display the events within the blue box in figure A-1b.

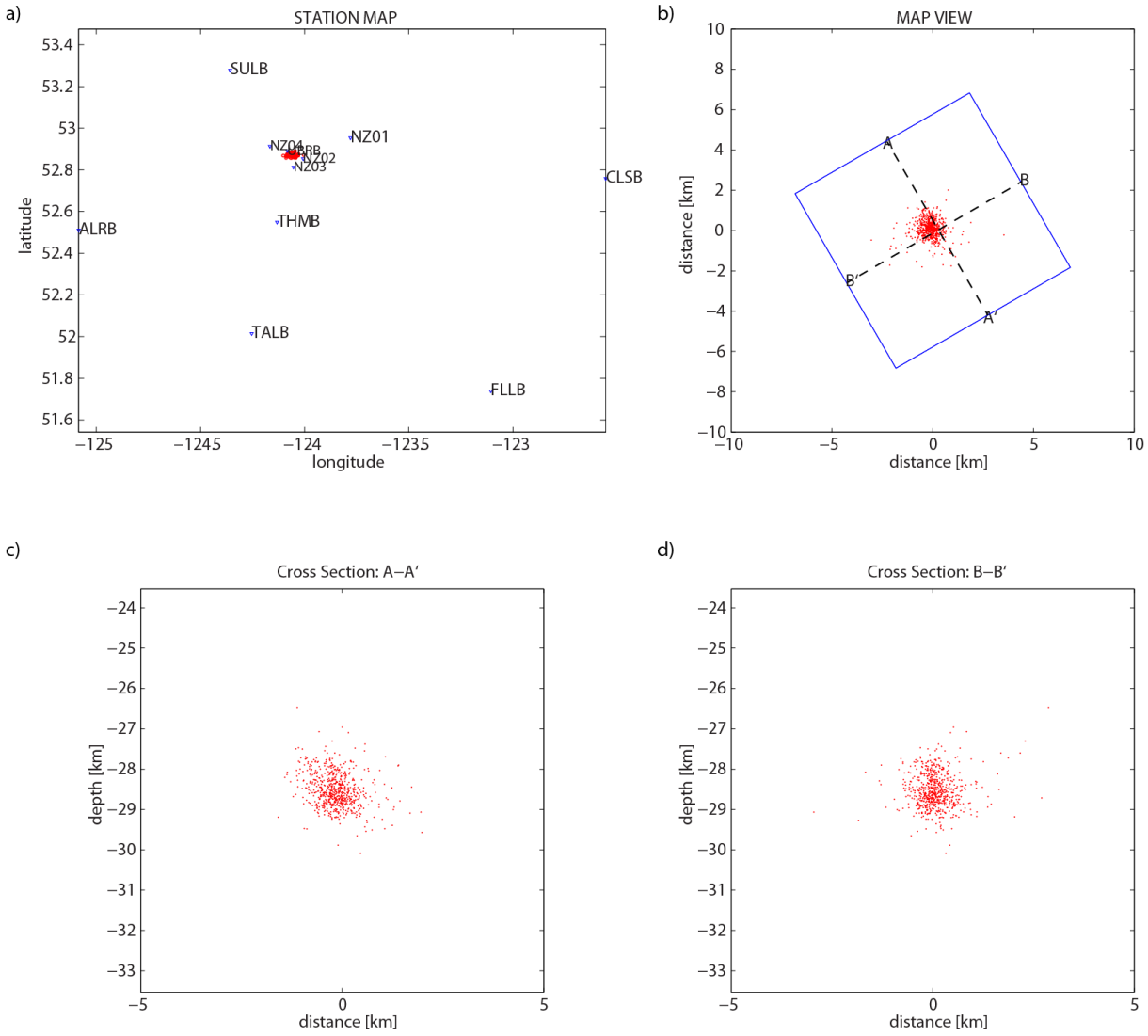

Figure A - 2. a) Epicentral relocations relative to the POLARIS and temporary stations. Relocations were calculated using HypoDD v. 1 and a catalog of cross-correlations with a coefficient of 0.7. b) Close-up view of epicenters. The section lines show the orientation of the cross sections in figures A-2c and A-2d below, which display the events within the blue box in figure A-2b.

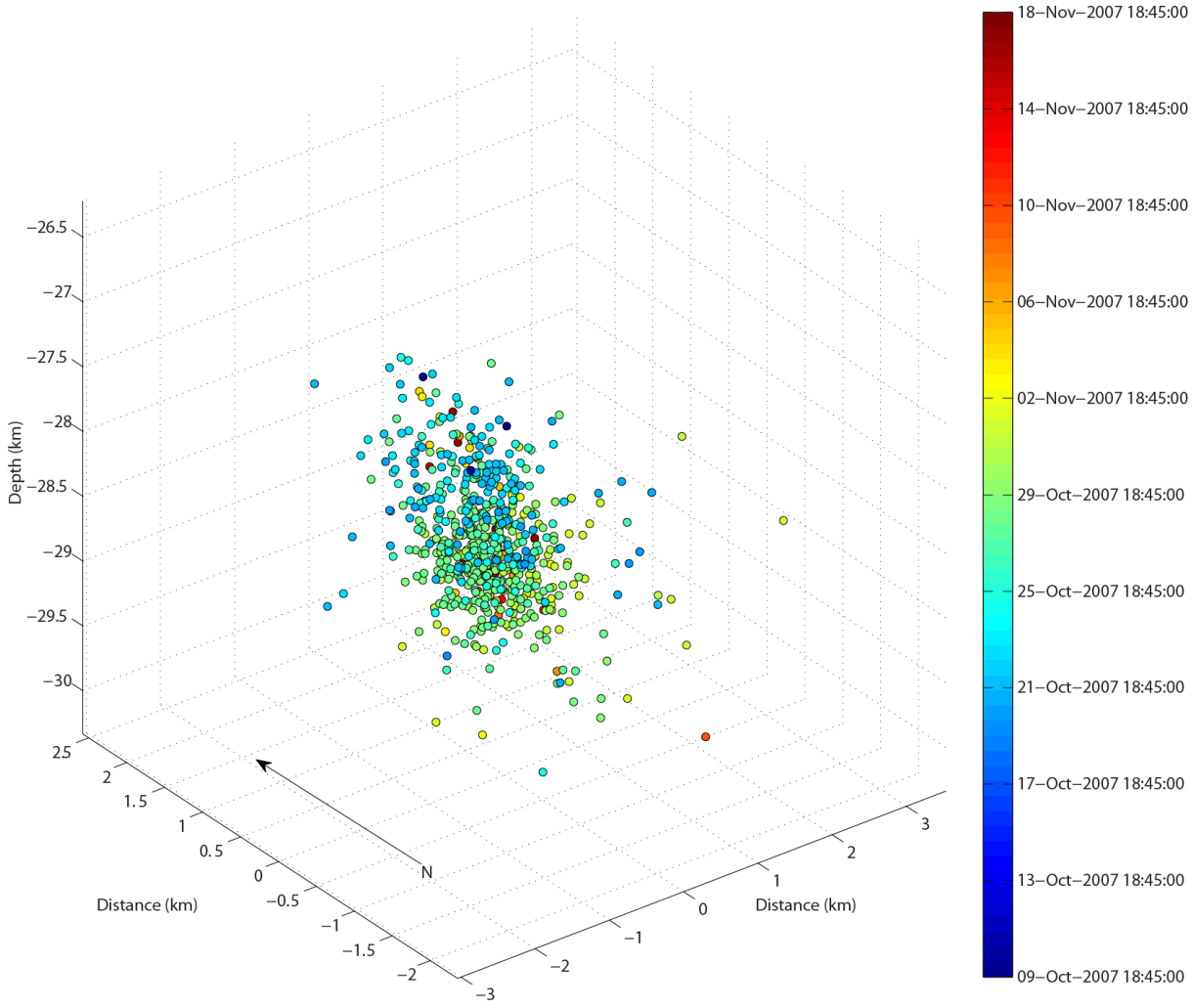

Figure A - 3. Time series plot of earthquakes relocated in HypoDD v. 1 (Figure A - 2). Cooler colors represent earlier activity and warmer colors represent the later stages of the swarm.

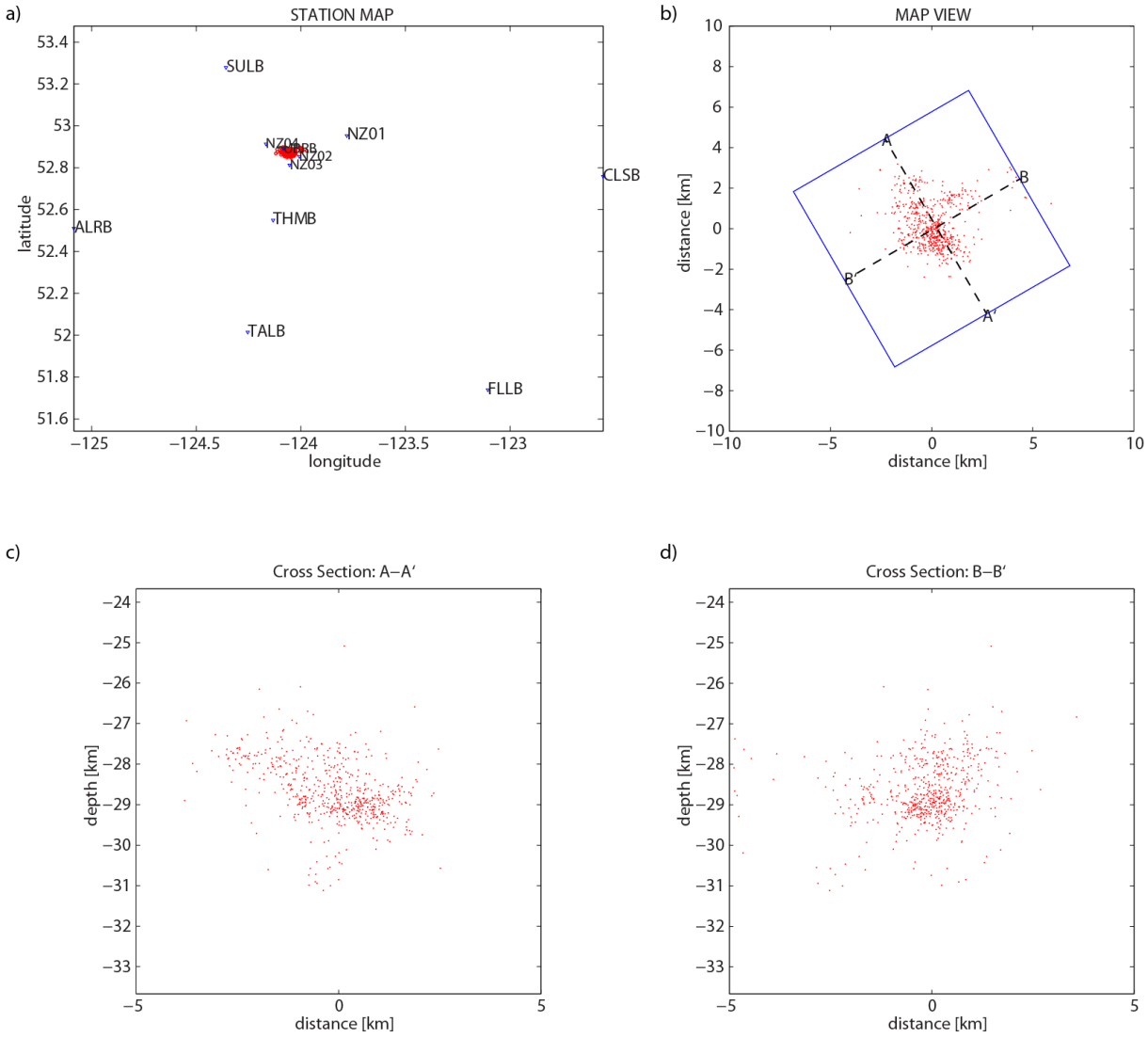

Figure A - 4. a) Epicentral relocations relative to the POLARIS and temporary stations. Relocations were calculated using TomoDD, a 3-dimensional velocity model derived from the model published by Cassidy et al. (2011), and a catalog of cross-correlations with a coefficient of 0.8. b) Close-up view of epicenters. The section lines show the orientation of the cross sections in figures A-4c and A-4d below, which display the events within the blue box in figure A-4b.

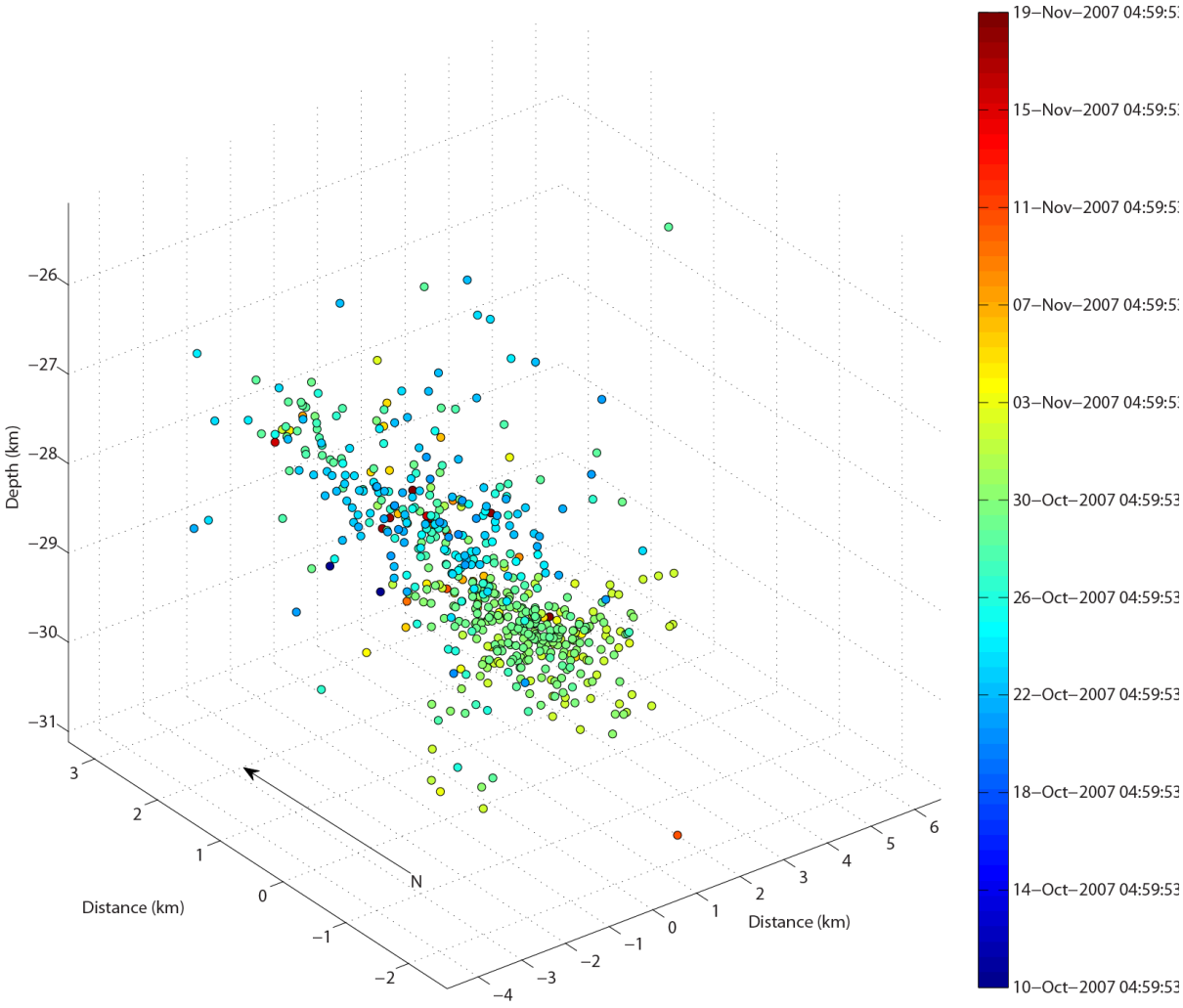

Figure A - 5. Time series plot of earthquakes relocated in TomoDD (Figure A - 4). Cooler colors represent earlier activity and warmer colors represent the later stages of the swarm.

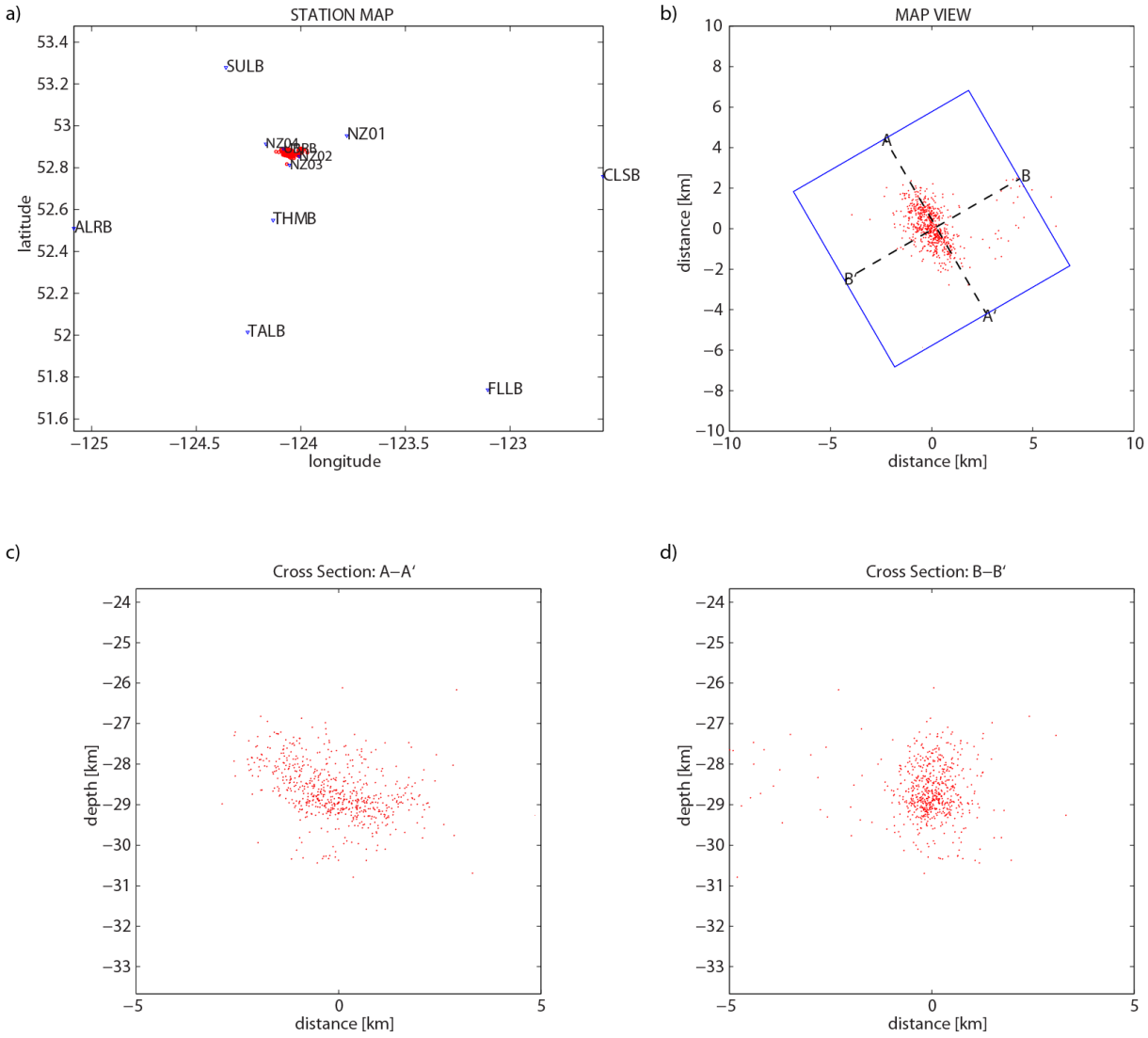

Figure A - 6. a) Epicentral relocations relative to the POLARIS and temporary stations. Relocations were calculated using TomoDD, a 3-dimensional velocity model derived from the model published by Cassidy et al. (2011), and a catalog of cross-correlations with a coefficient of 0.7. b) Close-up view of epicenters. The section lines show the orientation of the cross sections in figures A-6c and A-6d below, which display the events within the blue box in figure A-6b.